Journal of the Physical Society of Japan
Vol. 69, No. 9, September, 2000, pp. 3115-3132

Two-Dimensional Spectroscopy for Harmonic Vibrational Modes with Nonlinear System-Bath Interactions. I. Gaussian-White Case

Thomas STEFFEN and Yoshitaka TANIMURA[1,*]

Ultrafast Laser and Spectroscopy Laboratory, Department of Chemical Physics, University of Groningen, Nijenborgh 4, 9747 AG Groningen, The Netherlands
[1]*Institute for Molecular Science and the Graduate University for Advanced Studies, Myodaiji, Okazaki, Aichi 444-8585*

(Received April 6, 2000)

The quantum Fokker-Planck equation is derived for a system nonlinearly coupled to a harmonic oscillator bath. The system-bath interaction is assumed to be linear in the bath coordinates but quadratic in the system coordinate. The relaxation induced dynamics of a harmonic system are investigated by simulating the higher-order correlation functions of the Raman polarizability and the dipole moment, which represent the nonlinear optical responses of Raman or infrared spectroscopy. The 5th-order Raman response shows that, in addition to the frequency fluctuations induced by the bath, higher-order energy transfer between the system and bath plays a role. The nonlinearity of the system-bath interaction yields also an interesting feature in the 7th-order Raman echo or the 3rd-order infrared photon echo response: The calculations predict a finite signal for the case of a harmonic potential and a linear coordinate dependence of the polarizability or dipole while for linear system-bath coupling this response vanishes completely due to destructive interference of different Liouville space pathways.

KEYWORDS: 2D Raman, 2D IR, quantum Fokker-Planck, nonlinear system-bath interaction

§1. Introduction

Femtosecond nonlinear optical spectroscopies have proven to be valuable and versatile tools to obtain information on the dynamic characteristics of condensed phase systems.[1-6] Usually, these experiments are described by a response function formalism,[5,7] which is based on a perturbative expansion of the optical polarization in powers of the applied electric fields. For resonant spectroscopy, which is carried by the Infrared (IR) laser for molecular vibrational modes, the laser interaction is described by $\mu E(t)$, where μ is the dipole moment of the system. Then, for example, the lowest-order signal is expressed by the dipole correlation function $\langle\mu(t')\mu(t)\rangle$. For off-resonant Raman spectroscopy, in which resonance arises from a pair of laser pulses through Raman excitation processes, the laser interaction is described by $\alpha E^2(t)$, where α is the polarizability (Fig. 1). Since the Raman excitation requires a pair of pulses, the lowest-order Raman signal is third-order in the laser field including one probe field; it can be expressed by the correlation function of the Raman polarizability $\langle\alpha(t')\alpha(t)\rangle$. Higher-order optical responses are expressed by higher-order correlation functions of the dipole moment or the polarizability: The dynamic information of the Nth order resonant IR spectroscopy corresponds to the $(2N+1)$th-order off-resonant Raman spectroscopy.[5] However, it should be noted that the two types of experiments are governed by different selection rules for the transitions involved.

To calculate the (non)linear optical response one commonly assumes a certain functional form for the Hamiltonian of the medium, which allows for the derivation of closed form expressions that are fit to the experimental results. Such model approach, which is useful to understand the complex molecular interactions involved in optical processes, is complementary to more "realistic" approaches such as Molecular dynamics simulations. A typical example for this strategy is the Brownian oscillator model, which can be used to calculate, *e.g.*, the first-order resonant IR response or the third-order off-resonant Raman response.[5,8,9] Since the dipole moment or the polarizability is usually expanded in the power of molecular coordinate Q as $\mu(Q) = \mu_1 Q + \mu_2 Q^2 \cdots$ or $\alpha(Q) = \alpha_1 Q + \alpha_2 Q^2 \cdots$, the first-order IR or the third-order Raman response in lowest order of Q is nothing but the two-time correlation functions of Brownian

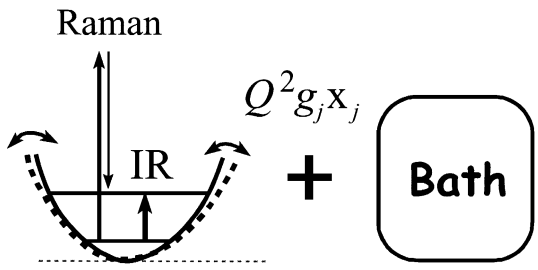

Fig. 1. Schematic view of a model system. A harmonic potential system is coupled to a heat bath system through a square-linear (SL) interaction, which causes the frequency modulation on the harmonic potential. In Raman spectroscopy, the resonance between vibrational levels arises from a pair of laser pulses through Raman excitation processes, whereas in IR spectroscopy, the resonance arises from an IR laser pulse.

* E-mail: tanimura@ims.ac.jp

oscillator $\langle[Q(t'), Q(t)]\rangle$. Correlation functions such as $\langle Q^2(t)Q^2(0)\rangle$ give rise to overtone transitions in conventional IR and Raman spectroscopy. Although models of vibrational and orientational dynamics can be tested against IR and Raman studies, there are still ambiguities. For example, one usually assigns the spectral density obtained from experiments to the spectral distribution of the harmonic oscillators (also called librators), but this may not be true for orientational dynamics because of the anharmonicity of the potential. In order to confirm the validity of models, one needs to have additional decisive experiments. Fifth-order two-dimensional Raman spectroscopy, which measures the two-time (three-point) correlation function of the polarizability $\langle[\alpha(Q(t'')), \alpha(Q(t')), \alpha(Q(t))]\rangle$, is such an example. It was proposed to experimentally separate the inhomogeneous distribution of slowly varying parameters, for example of local liquid configurations, from the total spectral density.[8] This experiment uses two pairs of excitation pulses, followed by a probe pulse and therefore has two time variables. By plotting the fifth-order signal as function of these delay times, we obtain the two-dimensional profile of the signal. Initial attempts to measure the 2D Raman response[10-12] underestimated the difficulties in suppressing cascading third-order contributions to the fifth-order signal.[13-16] The size of the unwanted cascading signals depends on the experimental geometry and on the coordinate dependence of the polarizability.[17] Recently, experimental progress has been made by optimizing the beam geometry and using diffractive optics.[18-20] The 2D information content of these time domain experiments can also be obtained from a frequency domain experiment.[21-24] By using narrow-band lasers (two IR excitation pulses, followed by one probe pulse which generates a Raman signal), Zhao and Wright demonstrated that such an experiment is indeed possible.[25-27] Resonant third-order experiments such as IR photon echoes[28-31] and two-dimensional IR[33-35] and nonresonant seventh-order experiments like the Raman echo[36-38] have been reported as well. Note that the 2D spectroscopy for electronically resonant experiments has also been proposed and has been carried out.[39-43]

The key to 2D optical experiments is the sensitivity of a profile to various dynamical information of molecules in condensed phases. It has been shown that fifth- and seventh-order 2D Raman experiments are useful to access for instance the degree of inhomogeneous broadening,[8, 44, 45] the anharmonicity of potentials and the nonlinearity of ploraziability,[46-53] the coupling mechanism between different vibrational modes[54-56] and the structural information of large molecules.[57, 58] In this paper, we calculate the third-, fifth- and seventh-order Raman responses, which correspond to the first-, second- and third-order responses of IR spectroscopy, for a harmonic system with a nonlinear system-bath interaction focusing on the mechanism of dephasing. Note that here we restrict our discussion to either Raman or IR spectroscopy, experiments that mix Raman and IR processes are also possible.[59]

Dissipation and dephasing phenomena, which are caused by complicated intra- and intermolecular interactions, can be incorporated at different levels of sophistication. In vibrational spectroscopies population and phase relaxation are often modeled by phenomenological level-dependent decay rates, that can be included in a perturbative treatment without major problems.[9, 60-63] However, these rates reflect the intermolecular dynamics in a rather indirect way, since they rely on the assumption of a white heat bath spectrum. Frequency fluctuations with a finite correlation time can be described by the stochastic model of Anderson and Kubo.[64-66] The dissipation of energy can be incorporated in the Brownian oscillator model by coupling the system to a set of harmonic oscillators.[5, 8, 67-70]

In this paper the nonlinear optical response is calculated by using the quantum Fokker-Planck equation,[71, 72] which has several advantages compared to the methods described above. To derive closed-form expressions for the response functions, one has to know the wavefunctions and transition matrix elements of the system Hamiltonian. Therefore, this strategy can be applied basically only to harmonic systems; the influence of small anharmonicities can then be treated by perturbation theory as was shown by Okumura and Tanimura.[46-48, 73] The quantum Fokker-Planck equation, on the other hand, can be used for potentials with an arbitrary shape and has been applied to Morse potentials[49] and displaced multistate systems.[74]

Moreover, this method allows for a sophisticated description of relaxation phenomena. For a Gaussian-Markovian heat bath with a finite correlation time, a hierarchy of equations of motions can be obtained from the spin-Boson Hamiltonian as was shown by Tanimura and Kubo.[75, 76] This technique allows for the description of a colored noise bath, but it extends the Kubo-Anderson model[65] by predicting an explicitly temperature dependent relaxation. Because it surpasses the traditional master equation approach, the hierarchy of equations of motions is often called doctor equation. Recently this method was applied to a harmonic oscillator and double-well potential,[77] tunneling of a quantum barrier in a dissipative system[78] and a three level system with Morse potential surfaces.[79, 80] Generalizations to arbitrary colored noise have also been studied.[81-83]

Up to now, the quantum Fokker-Planck approach has been applied only to systems, which were bilinearly coupled to a harmonic heat bath, also called linear-linear model (LL-model).[49, 71, 72, 77-83] The coupling of the system coordinate Q and the jth bath oscillator x_j by $H_{\rm SB} = c_j Q x_j$ describes energy relaxation out of the system into the heat bath as was first shown by Feynman and coworkers.[67] For harmonic potentials, linear coupling between the system and a continuous set of harmonic bath oscillators is, however, insufficient to induce pure dephasing. The loss of phase coherence can be achieved by anharmonicities in the system and/or bath potentials, or by a nonlinear coupling mechanism.[84] In the latter case the coupling of the system coordinate Q and the jth bath oscillator x_j is commonly described by an interaction Hamiltonian $H_{\rm SB} = g_j Q^2 x_j/2$ (Fig. 1). This coupling referred to as square-linear model (SL-

model) leads to pure dephasing as can be understood qualitatively by considering a harmonic coordinate Q, which can be expressed in terms of the creation and annihilation operators a and $a^\dagger$: The contributions proportional to $aa^\dagger$ and $a^\dagger a$ describe elastic random fluctuations of the frequency leading to a net loss of phase coherence without energy transfer to the heat bath.[85-89] Whether the linear or the quadratic coupling is more important for a particular system depends on the spectral density of the bath: When the density of states of the bath is high close to the system frequency, the energy transfer due to linear coupling can be very efficient. It has been shown for instance that the ultrafast relaxation of a solute molecule after electronic excitation can be described by the LL model; the strong coupling of different intra- and intermolecular modes to the transition coordinate leads to dominant rapid energy relaxation while pure phase relaxation is unimportant, see, *e.g.*, ref. 6. When the bath frequencies are much smaller than the system frequency, the resonant energy transfer is less efficient and the elastic fluctuation of the system frequency due to all bath oscillators can be dominant.[84] An example for this situation is found in vibrational relaxation: Often there is a big gap between the vibrational energy of a solute molecule and the vibrational states of the surrounding molecules. The phase coherence of solute molecules is then destroyed by nonresonant interactions between the solute and the solvent, which lead to fluctuations in the vibrational frequency of the solute.

Very recently, the SL model was investigated by Okumura and Tanimura, who used the Feynman rule on the unified-time path to derive a perturbative expression for the third-order Raman response.[90] In the limit of weak coupling they predicted a Lorentzian line shape for the spontaneous Raman line; the width of the line should scale linearly with temperature. At strong system-bath coupling their treatment is expected to break down because of the a^2 and $(a^\dagger)^2$ terms, which describe higher-order energy exchange between the system and the bath. As it will be shown below, the quantum Fokker-Planck approach confirms the third-order result of Okumura and Tanimura for weak coupling and demonstrates its breakdown for strong coupling. To further investigate the different relaxation processes due to this nonlinear system-bath interaction, we also calculate the fifth- and seventh-order Raman response. These temporally multidimensional techniques allow for an identification of different decay processes such as population relaxation and pure dephasing and therefore provide valuable additional insight in the system-bath interaction.[8-12, 37]

In §2 the quantum Fokker-Planck equation for quadratic coupling is presented and compared to the result for linear system-bath interaction.[71, 72] A derivation of this equation using the Feynman-Vernon path integral formalism[67-70] is given in the appendix. Calculational details of the simulations and examples for the wavepackets created in a fifth-order experiment are given in §3 and §4. The results for the first-, second-, and third-order IR response which are equivalent to the third-, fifth-, and seventh-order Raman response function are presented in §5 and §6, and finally conclusions are formulated in §7.

§2. The Quantum Fokker-Planck Equation for Nonlinear System-Bath Interaction

Since the early days of quantum mechanics the description of dissipation and relaxation phenomena has attracted much attention. Quantum mechanical Langevin and quantum master equations[65] have been applied to a large number of physical and chemical problems. However, these methods allow only for a perturbative treatment of the system-bath interaction and, therefore, they can be applied only in the limit of weak damping. In contrast to this, the functional integral description of dissipation, which was initiated by Feynman and Vernon,[67] can be applied to quantum systems at arbitrary temperature and coupling strength.[68]

In this section the quantum Fokker-Planck equation is introduced for the SL model and compared to the LL model.[71, 72] For both models the total Hamiltonian of the system and the bath can be written as:

$$H = \frac{P^2}{2M} + U(Q) + \sum_{j=1}^{N}\left[\frac{p_j^2}{2m_j} + \frac{m_j\omega_j^2}{2}\left(x_j - \frac{F_j(Q)}{m_j\omega_j^2}\right)^2\right]. \tag{1}$$

Here, Q, P, M and $U(Q)$ denote the effective coordinate, conjugated momentum, mass and the potential of the optically active degree of freedom, which is called the system. The coordinate, conjugated momentum, mass and frequency of the jth bath oscillator are given by x_j, p_j, m_j and ω_j, respectively. The coupling between the system and the jth bath oscillator is controlled by the function $F_j(Q)$ which is related to the system-bath interaction via: $H_{\rm SB} = -\sum x_j F_j(Q)$. In the LL model it is defined as $F_j(Q) = c_j Q$ while in the SL model it reads $F_j(Q) = g_j Q^2/2$. Note that the Hamiltonian of eq. (1) comprises a term proportional to $F_j(Q)^2$, which compensates for the coupling induced renormalization of the potential.[68, 71]

For the derivation of the quantum Fokker-Planck equation in the LL and the SL model one has to assume Gaussian white noise where the memory time of the heat bath is zero. The extension to a Gaussian-Markovian heat bath has been reported for the LL model[75-78] but this approach has not been applied to the SL model, yet. The spectral density of a Gaussian white bath $J(\omega)$ is given by the Ohmic distribution:

$$J_{\rm LL}(\omega) = \pi\sum_{j=1}^{N}\frac{c_j^2}{2m_j\omega_j}\delta(\omega-\omega_j) = M\zeta\omega, \tag{2}$$

and:

$$J_{\rm SL}(\omega) = \pi\sum_{j=1}^{N}\frac{g_j^2}{8m_j\omega_j}\delta(\omega-\omega_j) = M\zeta_{\rm SL}\omega. \tag{3}$$

It is further necessary to assume that the temperature of the bath is high, i.e., $\hbar\omega_0\beta \ll 1$ holds where ω_0 is the characteristic frequency of the system and $\beta = 1/k_{\rm B}T$.

The dynamics of the system and the bath can be de-

scribed by the coordinate representation $\rho_{\rm tot}(Q,\boldsymbol{x},Q',\boldsymbol{x}';t)\equiv\langle Q,\boldsymbol{x}|\rho_{\rm tot}(t)|Q',\boldsymbol{x}'\rangle$ of the time dependent density operator $\rho_{\rm tot}(t)$, where $\boldsymbol{x}$ denotes the coordinates of all N bath oscillators. The calculation of $\rho_{\rm tot}(Q,\boldsymbol{x},Q',\boldsymbol{x}';t)$ requires the exact knowledge of *all* degrees of freedom; for condensed phase systems this certainly has to be avoided. For the calculation of the system response due to, *e.g.*, external optical fields, it is sufficient to know the time evolution of this subsystem only, which is given by:

$$\rho(Q,Q';t)=\int {\rm d}\boldsymbol{x}\rho_{\rm tot}(Q,\boldsymbol{x},Q',\boldsymbol{x};t). \tag{4}$$

In the appendix the quantum Fokker-Planck equation for the SL model is derived by extending the treatment of Caldeira and Leggett[71] who investigated the LL model. Our treatment partly follows their paper, but deviates in a number of details. In particular, we start with a renormalized Hamiltonian which comprises a term proportional to $[F_j(Q)]^2$, and use modified effective coordinates to derive the equation of motion. Since for the derivation of the equation of motion the dynamics of the reduced density matrix has to be calculated, it is necessary to average out the bath degrees of freedom. For a harmonic bath the integration over the environment can be done analytically as was shown by Grabert and coworkers for bilinear system-bath coupling.[68] In the appendix it is demonstrated that this treatment is also possible for harmonic baths with system-bath interactions, which are linear in the bath coordinate, but nonlinear in the system coordinate. Grabert *et al.*[68] established that the system-bath interaction leads to a correlation between these two subsystems, even in thermal equilibrium. Initial conditions of the form $\rho_{\rm tot}(Q_i,\boldsymbol{x}_{\rm eq},Q_i',\boldsymbol{x}'_{\rm eq})=\rho(Q_i,Q_i')\rho_{\rm B}(\boldsymbol{x}_{\rm eq},\boldsymbol{x}'_{\rm eq})$, therefore, lead to unphysical results when these correlations are important, i.e., in the case of colored noise or a low temperature system. Since we will restrict ourselves to the high temperature Gaussian white noise case here, these problems do not affect our treatment.

The numerical calculations presented in the subsequent sections are performed in the Wigner representation, which relates the coordinate representation of the density matrix $\rho(Q,Q';t)$ to the phase space representation $W(P,R;t)$ via:[91-93]

$$W(P,R;t)=\frac{1}{2\pi\hbar}\int_{-\infty}^{\infty}{\rm d}r{\rm e}^{{\rm i}Pr/\hbar}\rho(R-r/2,R+r/2;t). \tag{5}$$

As was shown by Wigner and coworkers[91,93] the variables P and R can be associated with the momentum and the coordinate of the system.

The equation of motion for both the LL[49,71,72] and the SL model, i.e., the quantum Fokker-Planck equation, can be written as:

$$\frac{\partial}{\partial t}W(P,R;t)=-\mathcal{L}_SW(P,R;t)+\varGamma W(P,R;t). \tag{6}$$

Here, the free (undamped) propagation of the system is governed by:[94]

$$-\mathcal{L}_SW(P,R;t)=-\frac{P}{M}\frac{\partial}{\partial R}W(P,R;t)-\frac{1}{\hbar}\int\frac{{\rm d}P'}{2\pi\hbar}V(P-P',R)W(P',R;t), \tag{7}$$

where the Wigner representation of the potential $U(Q)$ is given by

$$V(P,R)=2\int_0^{\infty}{\rm d}r\sin(Pr/\hbar)[U(R+r/2)-U(R-r/2)]. \tag{8}$$

The relaxation in phase space is described by the damping operator, which in the LL model is given by:[49,71,72]

$$\varGamma_{\rm LL}=\zeta\frac{\partial}{\partial P}\left(P+\frac{M}{\beta}\frac{\partial}{\partial P}\right), \tag{9}$$

while in the SL model it reads:

$$\varGamma_{\rm SL}=4R^2\zeta_{\rm SL}\frac{\partial}{\partial P}\left(P+\frac{M}{\beta}\frac{\partial}{\partial P}\right)+R\zeta_{\rm SL}\hbar^2\frac{\partial^3}{\partial^2P\partial R}. \tag{10}$$

In presence of two independent baths for the two relaxation processes the total relaxation operator is $\varGamma=\varGamma_{\rm LL}+\varGamma_{\rm SL}$.

§3. Response Functions for Higher-Order Optical Processes

We now consider the optical measurements where the molecular system is interacting with a laser field, $E(t)$. For resonant IR spectroscopy, the Hamiltonian including laser interaction is given by

$$H_{\rm IR}=H-E(t)\mu(Q), \tag{11}$$

where $\mu(Q)$ is the coordinate dependent dipole moment. For off-resonant Raman spectroscopy, in which resonance arises from a pair of laser pulses through Raman excitation processes, the effective Hamiltonian is given by

$$H_{\rm Raman}=H-E^2(t)\alpha(Q), \tag{12}$$

where $\alpha(Q)$ is the coordinate dependent Raman polarizability. Since both dipole moment and Raman polarizability can be expanded by coordinate Q as $\mu(Q)=\mu_1Q+\mu_2Q^2\cdots$ or $\alpha(Q)=\alpha_1Q+\alpha_2Q^2\cdots$, the optical responses of resonant IR and Raman are formally identical besides the fact that the Nth-order IR spectroscopy corresponds to the $(2N+1)$th-order Raman spectroscopy. Note that "+1" arises from the probe pulse which induces the Raman signal. Therefore, hereafter we do not distinguish the Nth-order IR and $(2N+1)$th Raman processes and only present the results for Raman spectroscopy. Notice that the even-order of IR responses vanish for isotropic material, but they can be detected by using Raman process for the detection of signal.[25-27] This hints us to use both Raman and IR processes for higher-order spectroscopy.[59] This hybrid type of experiment has special advantages to study a coupling mechanism between Raman active and IR active modes. Theoretical basis is, however, identical to the pure Raman or IR case.

We consider the third-, fifth- and seventh-order Raman

experiments. The system first interacts with N pair of pulses for the $2N+1$th order optical process, which have the same time profile $E_j(t)$ ($j \leq N$). The last pulse $E_T(t)$ is the probe that generates the signal. The laser pulses are assumed to be impulsive and are configured for the (i) third-, (ii) fifth-, and (iii) seventh-order processes as (see Fig. 2)

$$\text{(i)} \quad E_1(t) = \delta(t), \quad E_T(t) = \delta(t - T_1)$$

$$\text{(ii)} \quad E_1(t) = \delta(t), \quad E_2(t) = \delta(t - T_1), \quad E_T(t) = \delta(t - T_1 - T_2)$$

$$\text{(iii)} \quad E_1(t) = \delta(t), \quad E_2(t) = \delta(t - T_1), \quad E_3(t) = \delta(t - T_1 - T_2), \quad E_T(t) = \delta(t - T_1 - T_2 - T_3). \tag{13}$$

The Raman signals are then expressed by the response functions as $I^{(2N+1)}(T_1, T_2, \ldots, T_N) = |R^{(2N+1)}(T_N, \ldots, T_2, T_1)|$, which are the N time correlation function of the polarizability operator $\alpha(Q)$. By introducing the Liouville space operator $\alpha^{\times}(Q)\rho \equiv \alpha(Q)\rho - \rho\alpha(Q)$ and the Liouville space Green function, $G(T) = \exp[-(\mathcal{L}_S - \Gamma)T]$,[8,9,49] they are expressed as

$$R^{(3)}(T_1) = \frac{\mathrm{i}}{\hbar}\langle\alpha(Q)G(T_1)\alpha^{\times}(Q)\rho(-\infty)\rangle, \tag{14}$$

$$R^{(5)}(T_2, T_1) = -\frac{1}{\hbar^2}\langle\alpha(Q)G(T_2)\alpha^{\times}(Q)G(T_1)\alpha^{\times}(Q)\rho(-\infty)\rangle, \tag{15}$$

and:

$$R^{(7)}(T_3, T_2, T_1) = -\frac{\mathrm{i}}{\hbar^3}\langle\alpha(Q)G(T_3)\alpha^{\times}(Q)G(T_2)\alpha^{\times}(Q)G(T_1)\alpha^{\times}(Q)\rho(-\infty)\rangle. \tag{16}$$

The processes corresponding to eqs. (14) to (16) can be depicted by double sided Feynman diagrams as was discussed in refs. 5, 8, 9 and 62 for different types of Raman response. Initially the equilibrium density matrix $\rho(-\infty)$ is modified by the first interaction, which yields a wavepacket $\rho_1 = \alpha^{\times}(Q)\rho(-\infty)$. This state is then propagated for a time T_1 by the Green function $G(T_1)$. In higher-order experiments the propagated density matrix is then modified again by the interaction and subsequently propagated. Finally, the expectation value of the observable polarizability is obtained by calculating the trace of $\alpha(Q)\rho_n$ where ρ_n denotes the density matrix after the last propagation period.

This sequence of modifying and propagating the density matrix can be translated very conveniently in the Wigner representation. The modified wavepacket in phase space W_1, which corresponds to the density matrix ρ_1, is given by:[49]

$$W_1 \equiv XW_{\mathrm{eq}} \equiv \int \frac{\mathrm{d}P'}{2\pi\hbar} X(P - P', R)W_{\mathrm{eq}}(P', R; -\infty), \tag{17}$$

where W_{eq} denotes the Wigner representation of the density matrix of the system in thermal equilibrium. The Wigner representation $X(P, R)$ of the operator $\alpha^{\times}(Q)$ is defined as:

$$X(P, R) = 2\int_0^{\infty} \mathrm{d}r \sin(Pr/\hbar)[\alpha(R - r/2) - \alpha(R + r/2)]. \tag{18}$$

The time evolution of the resulting wavepacket is obtained by numerically integrating eq. (6). For higher-order experiments the subsequent interactions are described by eq. (17) where now W_{eq} has to be replaced by the propagated wavepacket. The expectation value of the polarizability, which yields the signal after all interactions and propagation periods, is then given by:

$$tr\{A(P, R)W_n(P, R)\} \equiv \int \mathrm{d}P \int \mathrm{d}R A(P, R)W_n(P, R), \tag{19}$$

where $W_n(P, R)$ denotes the wavepacket after the last propagation period. The Wigner transform $A(P, R)$ of the polarizability operator $\alpha(Q)$ is given by:

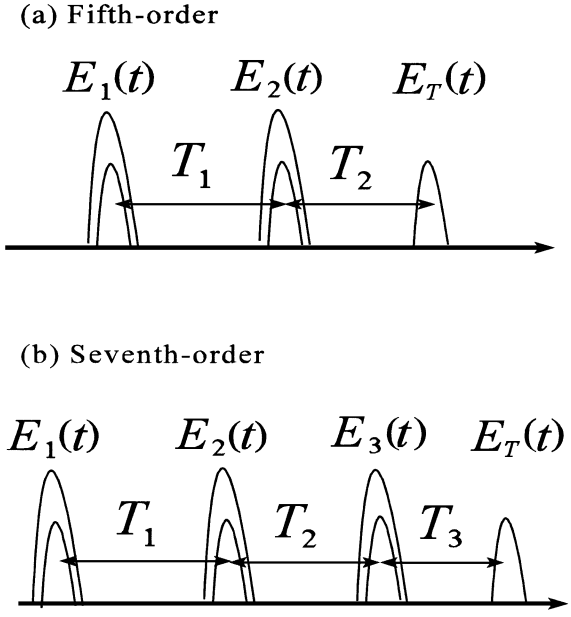

Fig. 2. Pulse configuration for (a) the fifth- and (b) the seventh-order off-resonant Raman experiments. Two or three pairs of pulses are applied to the system, which followed by the last probe pulse. In this paper, the temporal profiles of pulses $E_1(t)$, $E_2(t)$, $E_3(t)$ and $E_T(t)$ are assumed to be impulsive, i.e. $\delta(t - T_1 - T_3)$, $\delta(t - T_2)$, and $\delta(t)$ for (a), and $\delta(t - T_1 - T_2 - T_3)$, $\delta(t - T_2 - T_3)$, $\delta(t - T_3)$, and $\delta(t)$ with $T_2 = 0$ for (b).

$$A(P,R) = \mathrm{i}\int_{-\infty}^{\infty} \mathrm{d}r \mathrm{e}^{\mathrm{i}Pr/\hbar}\alpha(R-r/2), \qquad (20)$$

Using these equations, it is now possible to numerically simulate the third-, fifth-, and seventh-order response functions as will be explained in the next section.

§4. Wavepacket Dynamics in the Wigner Representation

In this section some details of the numerical calculations are given together with a description of the wavepacket dynamics in the Wigner representation. Hereafter, we employed dimensionless coordinate and momentum defined by $r \equiv R\sqrt{M\omega_0/\hbar}$ and $p \equiv P\sqrt{1/M\hbar\omega_0}$, respectively, where $\omega_0 \equiv \sqrt{U''(Q)/M}$. The simulations are performed for a harmonic mode with a frequency $\omega_0 = 38.7\,\mathrm{cm}^{-1}$ ($T = 1/\omega_0 = 861\,\mathrm{fs}$), which is a typical value for low-frequency intermolecular motions and which has been used in a previous study of a Morse potential.[49] Although the Fokker-Planck approach can be applied to any potential, we restrict ourselves in this pilot study to a harmonic coordinate, since different relaxation processes have been investigated for this system in great detail.[5, 8, 63, 67-72, 84-89] It is then in principle possible to solve the integral for the potential kernel [eq. (8)] analytically: the first term on the r.h.s of eq. (6) reduces to $1/2\omega_0 r\partial W/\partial p$. During the numerical calculations it turned out that the differential expression is less stable compared to the integral expression; therefore, the latter was used.

The quantum Fokker-Planck equation [eq. (6)] was numerically integrated on a discrete mesh in phase space using a second-order Runge-Kutta method. The mesh size was varied between 201×20 and 601×60 for mesh ranges between $-10 < r < 10$, $-15 < p < 15$ and $-15 < r < 15$, $-23 < p < 23$. The time steps for the finite difference expression $\partial W/\partial t$ were between 0.5 and 0.0125 fs. The accuracy of the calculations was checked by changing the mesh size, mesh range and time step size. On the mesh linear difference operators such as $\partial W/\partial r$ were approximated by $[W(p_i, r_{i+1}) - W(p_i, r_{i-1})]/(2\Delta r)$, whereas quadratic difference operators like $\partial^2 W/\partial r^2$ were replaced by $[W(p_i, r_{i+1}) - 2W(p_i, r_i) + W(p_i, r_{i-1})]/(\Delta r)^2$. The wavepacket W_{eq} in thermal equilibrium was generated numerically by starting with an initial wavepacket $W(p,r) = \exp[-\beta H_S(p,r)]$, where $H_S(p,r)$ denotes the Wigner transform of the undamped system Hamiltonian. After a short propagation period of typically a few thousand steps this wavepacket becomes stable.

The evolution of the wavepacket in a fifth-order temporally two-dimensional (2D) Raman experiment[8-12] is depicted in Fig. 3. In thermal equilibrium the wavepacket is symmetric and bell shaped as is shown in Fig. 3(a). In Fig. 3(b) the Wigner distribution is depicted directly after the first interaction. For this calculation the polarizability operator $\alpha(r)$ is expanded in powers of the coordinate up to second order, analogous to the treatment in refs. 8 and 9: $\alpha(r) = \alpha_1 r + \alpha_2 r^2$. The contribution due to the quadratic coordinate dependence of the polarizability is (almost) invisible since the coefficient of the linear contribution is chosen twenty times bigger than that of the quadratic contribution. Therefore, the distribution after the first interaction looks still symmetric in r but antisymmetric in p. This is completely analogous to the classical situation where the interaction $r^{\times}W_{\mathrm{eq}} \equiv [r, W_{\mathrm{eq}}]$ has to be replaced by $\{r, \rho_{\mathrm{eq}}\} = \partial r/\partial r\partial\rho_{\mathrm{eq}}/\partial p$. Note that in contrast to the classical density in phase space, $\rho(p,r)$, the Wigner distribution can be negative.[91-93]

This nonequilibrium distribution then starts to evolve in time due to the free propagator $\mathcal{L}_S$, which describes the periodic transfer of kinetic energy to potential energy and back: Those points in phase space with large positive (negative) momentum move in the positive (negative) r-direction while oscillators with zero momentum and a large positive (negative) deviation r turn back to acquire momentum. In other words, the wavepacket rotates in phase space with a frequency ω_0. In addition it changes its shape due to the damping operator Γ, which for the simulation shown here is chosen so small that the changes for small propagation times are minor. A snapshot of the propagated wavepacket is depicted in Fig. 3(c) for $T_1 = 200\,\mathrm{fs}$ corresponding to approximately a quarter of a period. Note that the part of the wavepacket close to the origin is slightly distorted as can be seen at the grid lines along p for small r, which already reflects the nonlinearity of the system-bath interactions. For the calculation of the third-order Raman response this propagated wavepacket has to be convoluted with the Wigner representation of the polarizability operator $A(p,r)$ and integrated over the entire grid, cf. eq. (19). In lowest order the third-order response is proportional to $[\alpha_1]^2$. The contributions due to the nonlinear coordinate dependence of the polarizability are very small.

In a 2D Raman experiment the propagated phase space distribution such as shown in Fig. 3(c) is modified by a second interaction operator X. The resulting wavepacket for a first propagation time of 200 fs is shown in Fig. 3(d). Analogous to the first interaction the symmetry of the wavepacket along the r-direction is not changed but it is inverted along the p-axis. This phase space distribution then evolves in time in a similar way as described above; a snapshot after a propagation time $T_2 = 200\,\mathrm{fs}$ is depicted in Fig. 3(e). Analogous to the calculation of the third-order Raman response the fifth-order response function is obtained by convoluting the propagated wavepacket after the second interaction with the Wigner representation of the polarizability operator $A(p,r)$, see also eq. (19).

In contrast to the third-order response, which is governed by the entire wavepacket and proportional to $[\alpha_1]^2$, the fifth-order signal is proportional to $[\alpha_1]^2[\alpha_2]$. Therefore, the latter is determined by the deformation of the wavepacket due to the small quadratic contribution. For the calculation of the temporally three-dimensional seventh-order Raman response the above described procedure has to be extended by an additional interaction and propagation period.

§5. Numerical Results

In this section the third-, fifth-, and seventh-order response functions of off-resonant Raman process, which are equivalent to the first-, second- and third-order re-

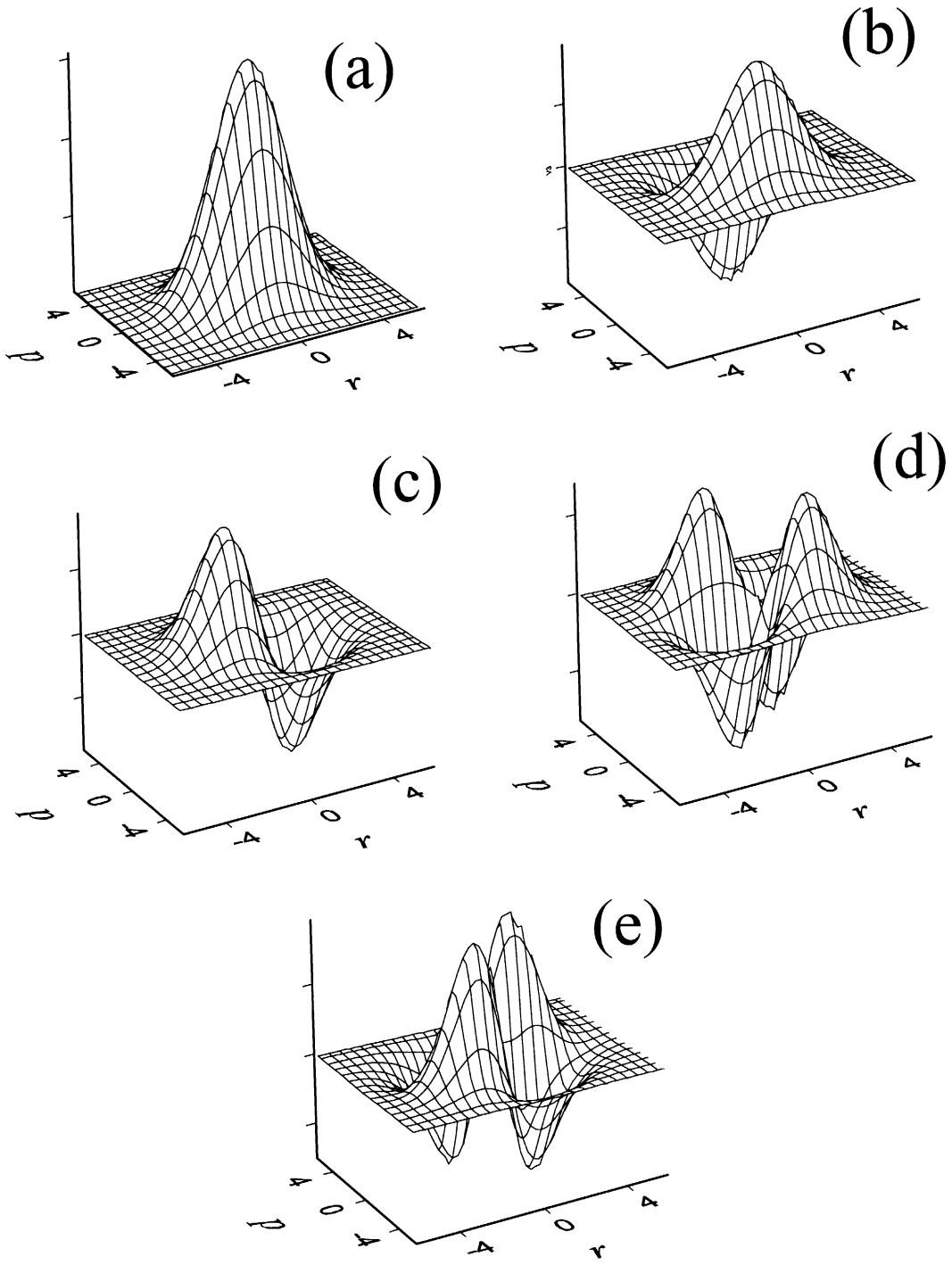

Fig. 3. The time evolution of the wavepacket in a 2D Raman experiment is shown for thermal equilibrium (a), directly after the first interaction at $T_1 = 0$ (b), at $T_1 = 200\,\mathrm{fs}$ (c), after the second interaction at $T_1 = 200\,\mathrm{fs}$ and $T_2 = 0$ (d) and at $T_2 = 200\,\mathrm{fs}$ (e). Consult text for details.

sponse function of IR process, are calculated for the SL model for different temperatures and coupling strengths. The results are compared to the LL model, which for Gaussian white noise and a harmonic system can be solved analytically.[8,9] In the LL model the line width is temperature-independent and there is no pure dephasing. The third-, fifth-order and seventh-order response function for $\alpha(r) = \alpha_1 r + \alpha_2 r^2$ are then in lowest order given by:[8,9]

$$R^{(3)}_{\mathrm{LL}}(T_1) = \frac{2\alpha_1^2}{\hbar} C''(T_1), \tag{21}$$

$$R^{(5)}_{\mathrm{LL}}(T_2, T_1) = \frac{4\alpha_1^2\alpha_2}{\hbar^2} C''(T_2)[C''(T_1 + T_2) + C''(T_1)], \tag{22}$$

and

$$R^{(7)}_{\mathrm{LL}}(T_3, 0, T_1) = \frac{16\alpha_1^2\alpha_2^2}{\hbar^3} C''(T_1)[C''(T_3)]^2, \tag{23}$$

where we have introduced the anti-correlation function of the Brownian oscillator

$$C''(t) \equiv \langle [Q(t), Q] \rangle = \frac{\omega_0}{\Omega} \mathrm{e}^{-\zeta|t|/2} \sin \Omega t, \qquad (24)$$

in which the reduced frequency Ω is defined as $\Omega = (\omega_0^2 - \zeta^2/4)^{1/2}$. When the polarizability depends only linearly on the coordinate, the seventh-order response function vanishes in the LL model due to perfect destructive interference of the Liouville space pathways involved.[8] For level-dependent damping, however, this interference can be (partly) destroyed, resulting in a finite signal as was discussed by Fourkas and coworkers.[62]

5.1 Third-order Raman signals (first-order IR signals)

In the SL model it is possible to derive a perturbative expression for the third-order response in the limit of weak damping, as was shown recently by Okumura and Tanimura.[90] They obtained the spontaneous off-resonant Raman line shape function $J(\omega)$, which looks similar to the one found in the LL model. The corresponding third-order response function is of the form of eq. (21), but in the SL model the effective damping constant ζ_{SL} and the overall intensity both scale linearly with the temperature. Because the calculations are quite complicated, the response for higher-order experiments has not been computed by this perturbation theory, yet.

As a reference, in Fig. 4 first we present the third-order signal for the LL model for different coupling strength $\zeta/\omega_0 = 0.1$, 0.5 and 1 calculated from eq. (21). In this case, the signal is the temperature independent. The spectral density displayed in the figure is the imaginary part of the Fourier transform of the third-order Raman response function,

$$R^{(3)}(\omega) = \int_0^\infty \mathrm{d}t \mathrm{e}^{\mathrm{i}\omega t} R^{(3)}(t), \qquad (25)$$

which is often used for the analysis of optically heterodyned detected optical Kerr effect data.[95-97] As can be seen from eq. (21) the peak position and width for the LL model are given by $\Omega = (\omega_0^2 - \zeta^2/4)^{1/2}$ and $\zeta/2$, respectively. Therefore the peak shifts to the red and becomes broader as the coupling ζ increases.

Figures 5 and 6 show the third-order results for the SL model for different temperature (T = 150, 300, and 450 for fixed $\zeta'/\omega_0 = 0.025$) and coupling strength ($\zeta'/\omega_0 = 0.01$, 0.1, and 0.5 for fixed $T = 300\,\mathrm{K}$, where we set $\zeta' = \hbar\zeta_{\mathrm{SL}}/m\omega_0^2$.) In Fig. 5, the third-order results of the quantum Fokker-Planck simulation are compared to the predictions of the theory by Okumura and Tanimura.[90] For weak coupling the line width increases linearly with temperature and the two methods agree very well. This temperature dependence is expected because of the nonlinear coordinate dependence of the damping operator Γ_{SL} [see eq. (10)]: As the temperature is increased, the wavepacket becomes broader and in particular the outer parts of the wavepacket are damped more strongly. With increasing damping the perturbation theory breaks down as is shown in Fig. 6. When $\zeta'/2$ is bigger than ω_0, the line shape becomes bimodal: In addition to a broad feature around ω_0 there is a (nearly) Lorentzian peak close to zero frequency. In time domain this feature, which is also found in the OHD-OKE response of many molecular liquids[95-97] shows up as an exponential decay.

The physical origin of the bimodal structure at strong damping can be understood qualitatively from the form

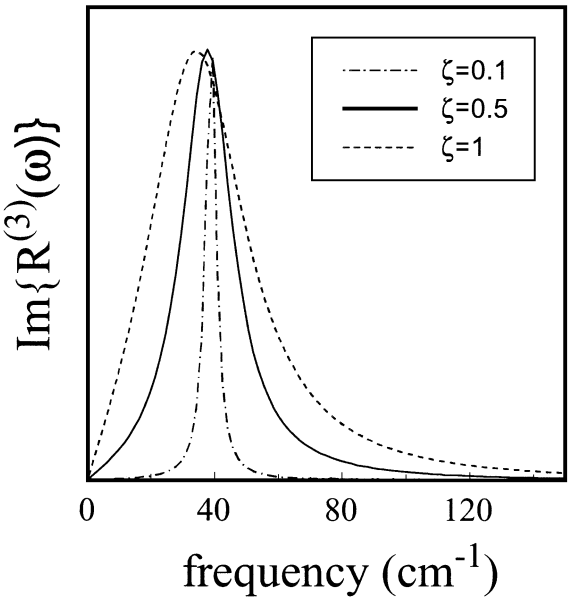

Fig. 4. The spectral density of the third-order Raman response of a harmonic mode in the LL-model for $\zeta/\omega_0 = 0.1$ (dashed-dotted), 0.5 (solid line) and 1.0 (dashed). Note that the results for the LL model are the temperature independent.

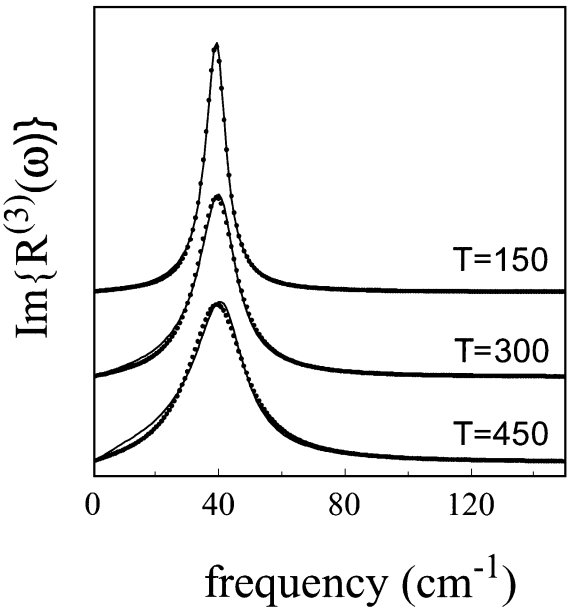

Fig. 5. The spectral density of the third-order Raman response of a harmonic mode in the SL-model for T = 150, 300 and 450 K (bottom to top) calculated by the quantum Fokker-Planck equation (solid line) and by the perturbation theory of Okumura and Tanimura (dotted). The frequency of the undamped mode is $\omega_0 = 38.7\,\mathrm{cm}^1$, the damping constant ζ' was equal $0.025\omega_0$.

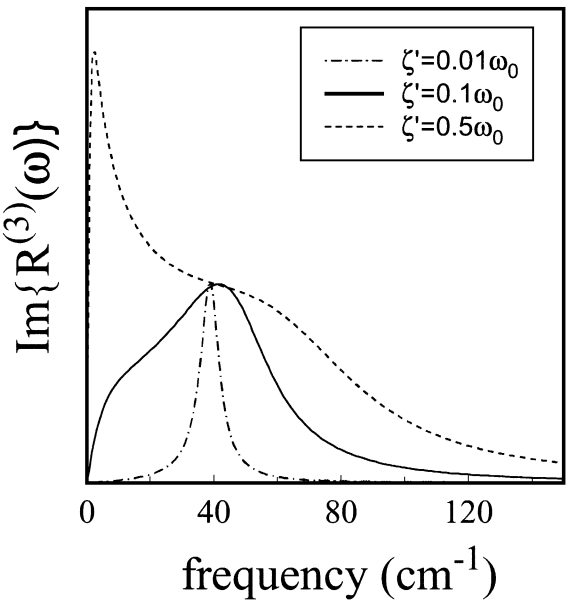

Fig. 6. The spectral density of the third-order Raman response of a harmonic mode in the SL-model at the temperature $T = 300\,\mathrm{K}$ for $\zeta/\omega_0 = 0.01$ (dashed-dotted), 0.1 (solid line) and 0.5 (dashed).

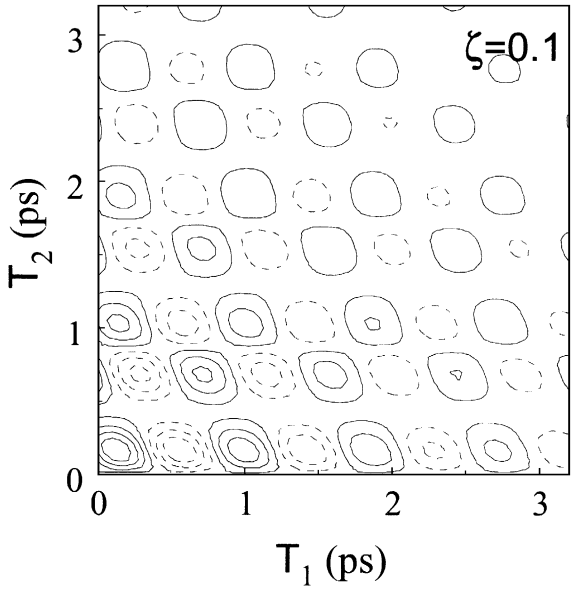

Fig. 7. Contour plot of the fifth-order Raman signal $I^{(5)}(T_1, T_2) = R^{(5)}(T_2, T_1)$ in the LL-model for $\zeta/\omega_0 = 0.1$. Dashed contours are negative. We set the nonlinear polarizability $\alpha_2 = 0.01\alpha_1$.

of the system-bath coupling $H_{\mathrm{SB}} = -g_j Q^2 x_j$. When expressed in terms of the creation and annihilation operators of the system, a and $a^\dagger$, one directly sees that in addition to pure dephasing due to the coupling terms proportional to $aa^\dagger$ and $a^\dagger a$ there is also energy exchange between the system and the bath via the terms a^2 and $[a^\dagger]^2$. Analogous to the LL model, the energy relaxation will lead to the large red peak shift for strong coupling, whereas the pure dephasing will not change the peak position regardless of the coupling strength. If two types of the relaxation processes play a role at once, we thus observe the bimodal structure for strong coupling.

5.2 Fifth-order Raman signals (second-order IR signals)

In order to better distinguish the effects of population and phase relaxation it is instructive to investigate the fifth-order Raman response, which due to its temporally two-dimensional character provides additional insight. In the following, we plot the fifth-order response function, $R^{(5)}(T_2, T_1)$, which corresponds to the signal for impulsive excitation and heterodyne detection.[98] As a reference, in Fig. 7 we present the fifth-order signal for the LL model in weak coupling case $\zeta = 0.1\omega_0$ calculated from eq. (22). As can be seen from eq. (22) the period in the T_1 direction is $1/2\Omega \approx 0.4\,\mathrm{ps}$ (note that dashed contours are the negative part). On the other hand, the period in the T_2 direction is determined by the interference of the oscillations with the period $1/2\Omega$ and $1/\Omega$ (remember that $\sin. T_2[\sin\Omega(T_1 + T_2)] = [\cos\Omega(T_1 + 2T_2) - \cos\Omega T_1]/2$), resulting in twin peaks with a period of $1/\Omega = 0.8\,\mathrm{ps}$.

Figures 8 and 9 show the fifth-order signal $I^{(5)}(T_1, T_2) = R^{(5)}(T_2, T_1)$ for the SL model for different temperatures ($T = 450$, 300, and 150 K for fixed $\zeta'/\omega_0 = 0.025$) and coupling strengths ($\zeta'/\omega_0 = 0.01$, 0.1 and 0.5 for fixed $T = 300\,\mathrm{K}$), respectively. For a weak coupling and a low bath temperature the 2D Raman response function $R^{(5)}(T_2, T_1)$ exhibits clear oscillations with the frequency ω_0 as is shown in Fig. 8(c). For weak coupling, the fifth-order signals also show twin peaks for all temperatures, however, the phase in T_2 direction is different from the LL model, Fig. 7. A similar feature is found in Fig. 7(c) of ref. 66, which shows the fifth-order response of a harmonic oscillator in the fast fluctuation (homogeneous) limit of the stochastic model. In this limit the dynamics is due to pure dephasing with a level dependent rate constant $\Gamma_{\lambda\mu} = (\lambda - \mu)^2\Gamma^*$ where λ and μ are the quantum numbers of the involved states and Γ^* denotes the pure dephasing rate constant. This indicates that for small ζ' the SL model describes pure dephasing.

For large ζ' the fifth-order response is distinctly different as is shown in Fig. 9(c): As function of the first delay time T_1 the fifth-order signal rapidly decays within a few hundred fs, while along T_2 it shows slow diffusive dynamics on a ps time scale. This asymmetry of the 2D Raman response can be understood by considering the Liouville space pathways involved: In all Liouville space pathways contributing to the fifth-order 2D Raman response the system first propagates in a coherence, which rapidly decays due to the strong coupling ζ'. As was discussed in ref. 9, the fifth-order response comprises one contribution proportional to $\cos\omega T_1$, which involves a population during the second propagation time. In the limit of pure dephasing this term does not decay at all and yields a plateau along T_2 for small T_1, as was also found in Fig. 7 of ref. 9. In the SL model, however, the signal does decay as function of T_2 when ζ' is large [see Fig. 9(c)]. The underlying population relaxation is induced by two quantum transitions between the system

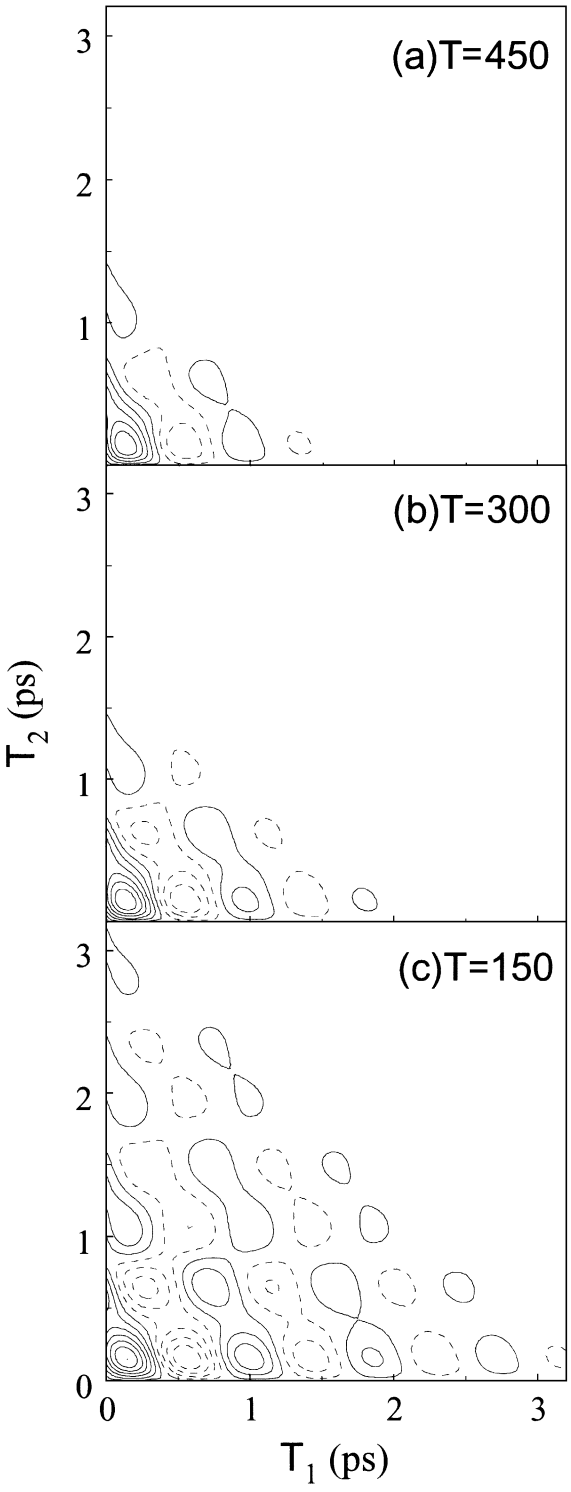

Fig. 8. Contour plot of the fifth-order Raman signal $I^{(5)}(T_1, T_2) = R^{(5)}(T_2, T_1)$ in the SL-model for $\zeta' = 0.025\omega_0$ at different temperature at (a) $T = 450$, (b) $T = 300\,\mathrm{K}$, and (c) $T = 150\,\mathrm{K}$. Dashed contours are negative. We set the nonlinear polarizability $\alpha_2 = 0.01\alpha_1$.

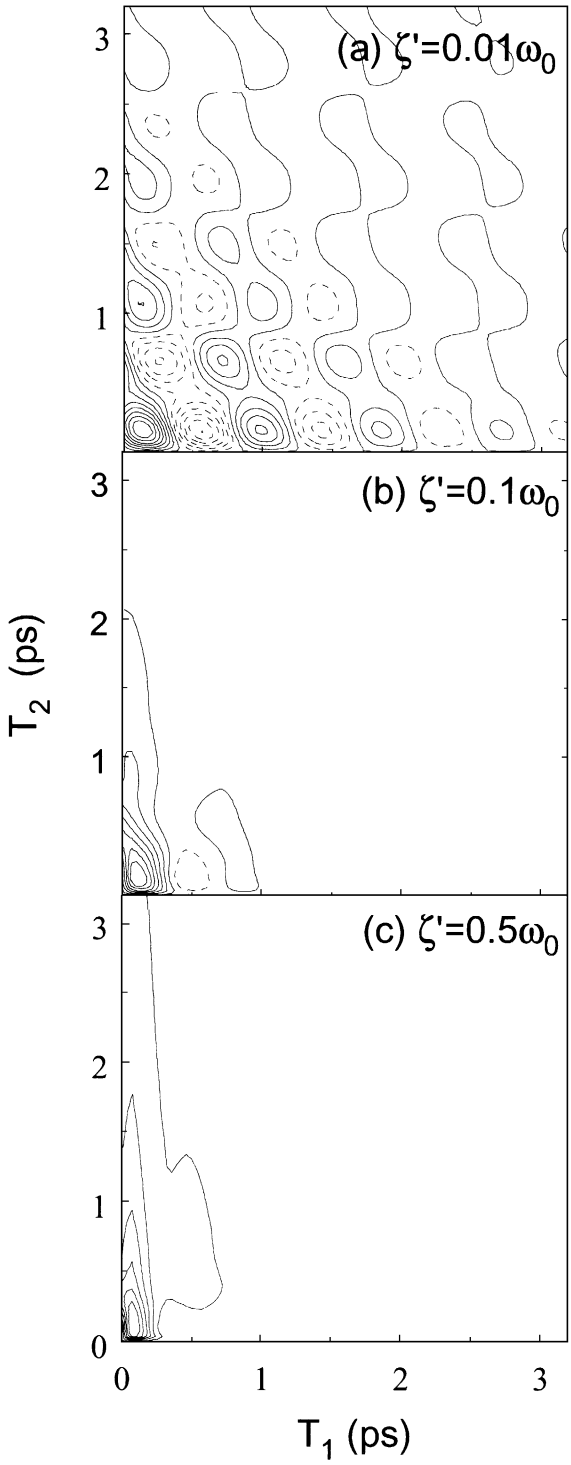

Fig. 9. Contour plot of the fifth-order Raman signal $I^{(5)}(T_1, T_2) = R^{(5)}(T_2, T_1)$ in the SL-model at $T = 300\,\mathrm{K}$ for different coupling strength (a) $\zeta' = 0.01\omega_0$, (b) $\zeta' = 0.1\omega_0$, and (c) $\zeta' = 0.5\omega_0$. Dashed contours are negative. We set the nonlinear polarizability $\alpha_2 = 0.01\alpha_1$.

and the bath, which are due to the coupling terms proportional to a^2 and $[a^\dagger]^2$.

5.3 Seventh-order Raman signals (third-order IR signals)

The nonlinear character of the relaxation in the SL model becomes also evident in the seventh-order response or, equivalently, the third-order IR response. In the LL model the seventh-order response function vanishes when the polarizability depends only linearly on the coordinate because the different Liouville space pathways interfere destructively.[8,62] This reflects the fact that the leading term in eq. (23) is not α_1^4 but $\alpha_1^2\alpha_2^2$. The LL model is a linear problem, which can be diagonalized

and, therefore, there is no nonlinear response. When the damping is level-dependent, the interference can be partly destroyed and the seventh-order response is finite even for a linear coordinate dependence of the polarizability.[62] In the SL model the damping operator $\Gamma_{\rm SL}$ has a large nonlinear contribution in r, see eq. (10), and one, therefore, can expect a finite response. The impulsive seventh-order Raman response function [eq. (16)] is temporally three-dimensional but up to now only temporally two-dimensional seventh-order experiments have been performed. In the Raman echo the second propagation time T_2 is zero whereas in the Raman pump probe experiment the time variable T_1 is zero.[37,99,100] Note that in IR spectroscopy, the former case corresponds to the IR photon echo experiment.[28-31,34] In this study we set T_2 to zero to compare our results with the echo experiments. We should notice that due to the anharmonicity of the molecular vibrations, the transitions to higher vibrational states were not resonant with the applied ps pulse. The seventh-order Raman and third-order IR experiments reported so far were done nonimpulsively on a two level system.

In the following, we plot the seventh-order response, $I^{(7)}(T_1,T_3) = R^{(7)}(T_3,0,T_1)$. We first present the signal for the LL model in Fig. 10. The coupling strength is chosen as $\zeta/\omega_0 = 0.1$. This result is also temperature independent. As can be seen from eq. (23) the signal is also asymmetric, because $\sin^2 \Omega T_2 \propto \sin 2\Omega T_2$.

Figures 11 and 12 show the seventh-order signal for the SL model for different temperatures ($T = 150$, 300, and 450 for fixed $\zeta'/\omega_0 = 0.025$) and coupling strength ($\zeta'/\omega_0 = 0.01$, 0.1, and 0.5 for fixed $T = 300\,\mathrm{K}$). The parameters are chosen to be the same as Figs. 8 and 9. As mentioned before the leading order of the signal in the SL case is α_1^4, whereas the LL case is $\alpha_1^2\alpha_2^2$. This indicates that although some profiles in SL model are similar to Fig. 10, the origin of the signal is very different. This also indicates that even though the fifth-order signal, which is proportional to $\alpha_1^2\alpha_2$ in both the LL and SL case, is very weak due to the small nonlinearlity $\alpha_2 \ll 1$, the seventh-order signal may be strong for the SL case.

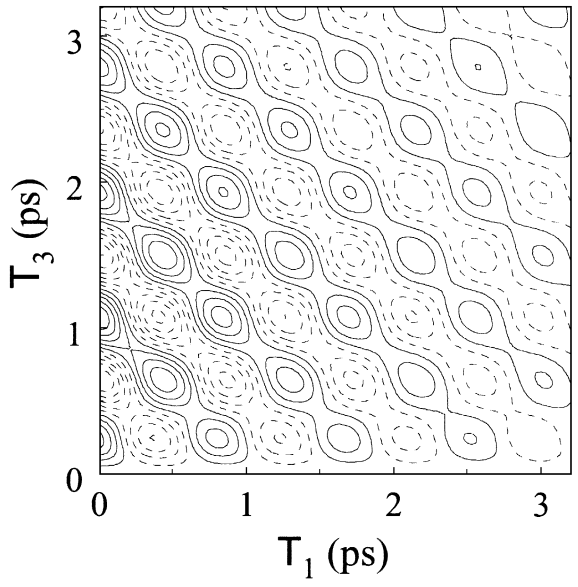

Fig. 10. Contour plot of the seventh-order Raman signal $I^{(7)}(T_1,T_3) = R^{(7)}(T_3,0,T_1)$, in the LL-model for $\zeta/\omega_0 = 0.1$. Dashed contours are negative. We set the nonlinear polarizability $\alpha_2 = 0.01\alpha_1$.

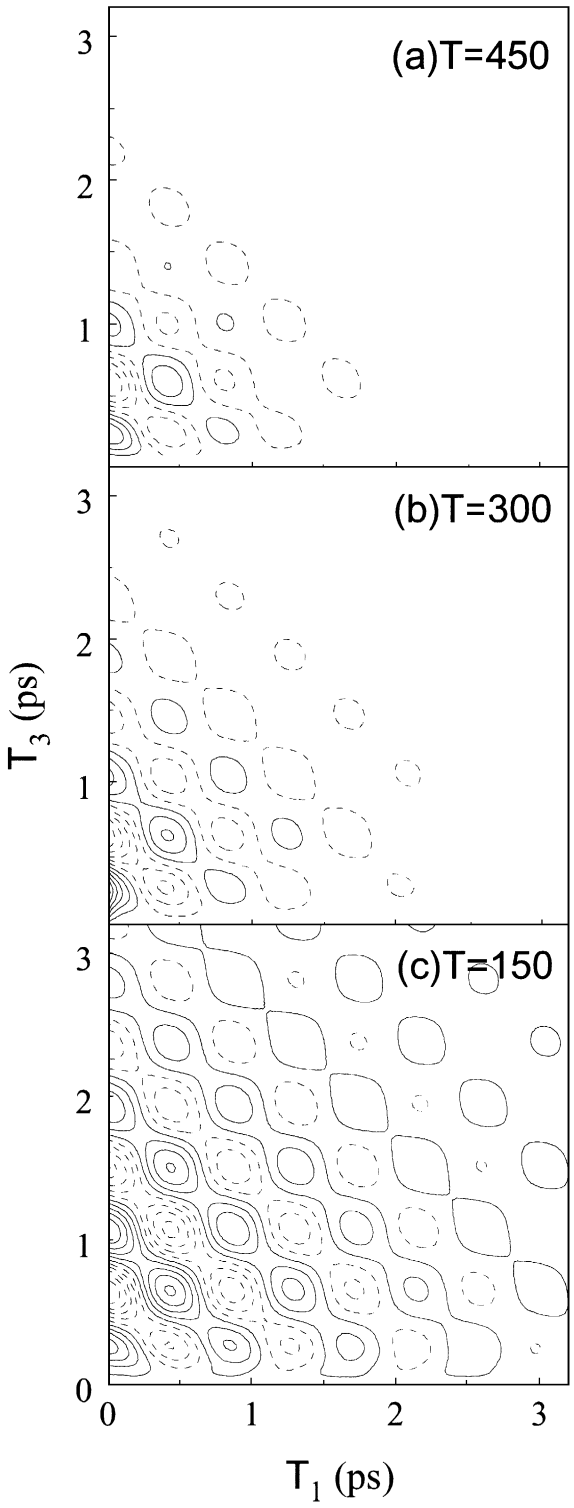

Fig. 11. Contour plot of the seventh-order Raman signal $I^{(7)}(T_1,T_3) = R^{(7)}(T_3,0,T_1)$ in the SL-model for $\zeta' = 0.025\omega_0$ at different temperature at (a) $T = 450$, (b) $T = 300\,\mathrm{K}$, and (c) $T = 150\,\mathrm{K}$. We set the nonlinear polarizability $\alpha_2 = 0.0$. Dashed contours are negative.

In the limit of low temperature (but $\beta\hbar\omega_0 \ll 1$) and weak coupling, Fig. 11(c) or 12(a), the response shows clear oscillations with frequency ω_0 that slowly decay. A similar behavior is found in the model of Fourkas and coworkers[62] who calculated the seventh-order response for level dependent population and phase relaxation. For strong coupling, Fig. 12(c), the response changes quite significantly: The signal decays more rapidly and the oscillation frequency becomes *higher*. Note that in the LL model the reduced frequency becomes smaller as the damping strength is increased. In the SL model, the bath interaction modulates the system frequency and thus the coupling strength between the system and bath increases the system frequency. Damping can be stronger, since the energy exchange between the system and the bath via the terms a^2 and $[a^\dagger]^2$ is more effective than the a and $a^\dagger$ in LL model case.

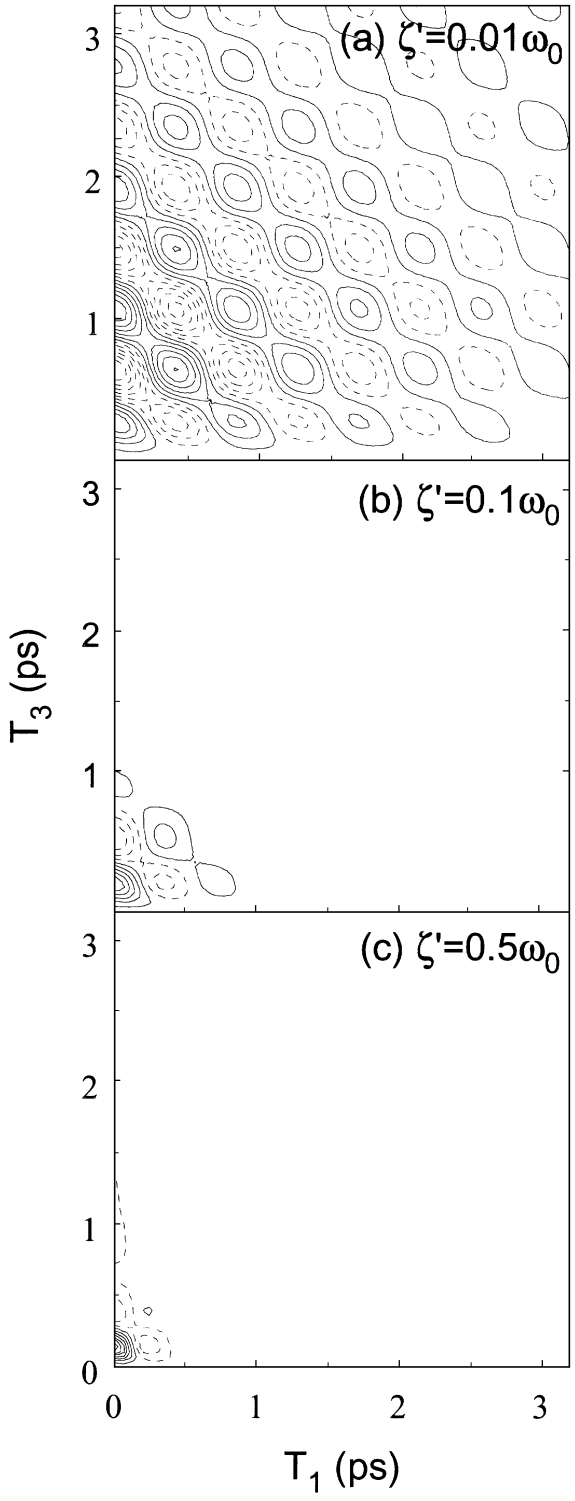

Fig. 12. Contour plot of the seventh-order Raman signal $I^{(7)}(T_1, T_3) = R^{(7)}(T_3, 0, T_1)$ in the SL-model at $T = 300\,\mathrm{K}$ for different coupling strength (a) $\zeta' = 0.01\omega_0$, (b) $\zeta' = 0.1\omega_0$, and (c) $\zeta' = 0.5\omega_0$. Dashed contours are negative.

Neither of plots in Figs. 11 and 12 shows an echo feature at the diagonal $T_1 = T_2$, which would be expected for an inhomogeneously broadened two-level system.[36] Since the spectral density $J(\omega)$ of eq. (3) is chosen for the case of Gaussian white noise, one can indeed anticipate that the memory time of the system is zero and that there is no echo. The effect of a finite correlation time of the bath fluctuations can be described, in principle, by the theory of Tanimura and Kubo[75-79] but this approach has not been applied, yet, to the SL model. We will discuss it in the next paper.[101]

§6. Frequency domain experiments

The signal we presented in §5 is induced Raman signal or IR intensity. These signals are equivalent to the response function itself. If we perform the Fourier transformation of signals:

$$R^{(n)}(\omega_2, \omega_1) = \int_0^\infty \mathrm{d}t_1 \int_0^\infty \mathrm{d}t_2 \mathrm{e}^{\mathrm{i}\omega_1 t_1 + \mathrm{i}\omega_2 t_2} R^{(n)}(t_2, t_1) \tag{26}$$

for $n = 5$ or 7, we can carry out more detailed analysis based on the frequency. It was shown that by using frequency domain experiment instead of the time domain, one can directly obtain the frequency domain information eqs. (26).[21] Wright, *et al.* carried out such frequency domain experiments by using two tunable IR laser and one set of Raman detection pulse.[25-27] Here, we present the 3D profiles of bare response functions $R^{(n)}(T_2, T_1)$ and absolute value of their Fourier transformation $I^{(n)}(\omega_2, \omega_1) = |R^{(n)}(\omega_2, \omega_1)|$.

Figs. 13 and 14 show the profiles of the fifth- and seventh-order response functions for (a) the harmonic LL case, and (b) the SL case and the absolute values of their double Fourier transformation (a′) and (b′). To calculate the response functions we set $T = 150\,\mathrm{K}$ and $\zeta/\omega_0 = 1$ for (a) and (a′), and $\zeta'/\omega_0 = 0.5$ for (b) and (b′). Compared with the time-domain results Figs. 13(a) and 13(b), we can easily observe the change of the resonant frequency in Figs. 13(b) and 13(b′). In the LL case (a) the peaks shift to the red (small frequency) in both ω_1 and ω_2 direction, since the peak frequency is determined by $\Omega = (\omega_0^2 - \zeta^2/4)^{1/2}$ and Ω becomes small for large ζ as was observed in Fig. (3). In the SL case (b′), on the other hand, the peaks shift to the blue (large frequency), since the SL model induces the modulation on the system frequency and therefore the effective frequency becomes large when the coupling becomes strong. In Fig. 13(b′), we also observe the central peak at $(0, 0)$, which were originated from the energy relaxation via the terms a^2 and $[a^\dagger]^2$ discussed as the bimodal structure

of the third-order signal in Fig. 4. Figure 14 shows the seventh-order signal. As was seen in the fifth-order case, we observe the peaks shift to the red in the LL model whereas the blue in the SL model. Although the profile of (a) and (b) are somewhat similar, the signal for (a) is proportional to the polarizability ($\alpha_1^2\alpha_2^2$) and that for (b) is proportional to the (α_1^4). Therefore the intensity of signals (a) and (b) can be very different especially for small α_2.

§7. Conclusions

The quantum Fokker-Planck equation is derived for a system that is nonlinearly coupled to a heat bath. In the SL model studied here, it is assumed that the system-bath interactions are linear in the bath coordinate but quadratic in the system coordinate. The equation of motion for the wavepacket in Wigner space is solved numerically which allows for the calculation of the third-, fifth-, and seventh-order Raman response of a harmonic oscillator with (non)linear coordinate dependence of the polarizability. For weak coupling the third-order response function can be modeled by the perturbation theory of Okumura and Tanimura.[90] In the SL model the width of the third-order Raman line scales linearly with the temperature while it is temperature independent in the LL model. When the system and the bath are strongly coupled, the third-order response becomes bimodal: Next to the original line there is a Lorentzian line close to zero frequency, which is not present in the perturbation theory. This line is attributed to two-quantum energy transfer from the system to the bath, which is described by the coupling terms proportional to a^2 and $[a^\dagger]^2$.

The contributions of energy and phase relaxation can be disentangled in the fifth-order 2D Raman response. For weak coupling the neighboring maxima of the 2D Raman response form twins; a feature that was also found

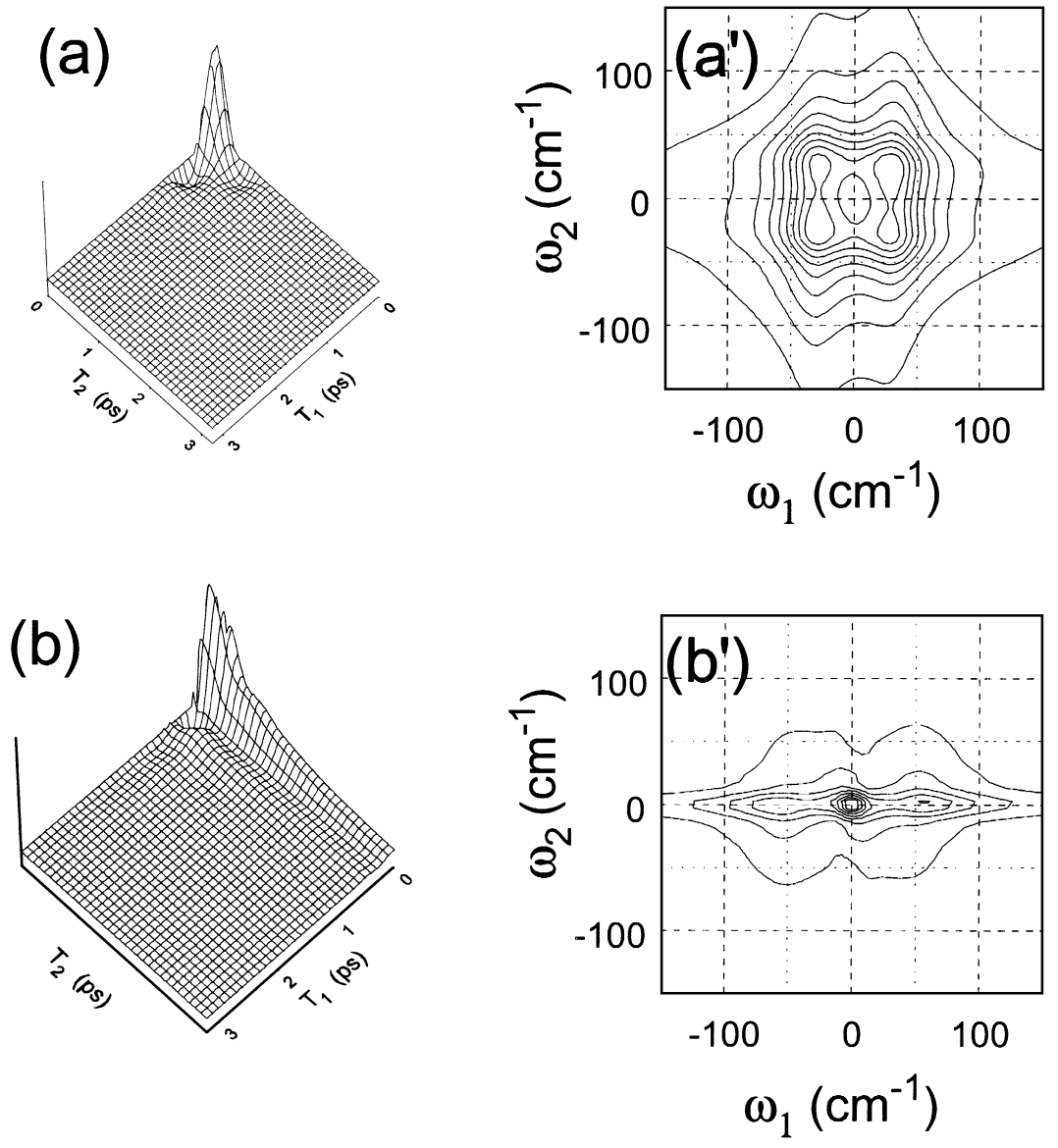

Fig. 13. Three-dimensional profile of the fifth-order Raman signal $I^{(5)}(T_1, T_2) = R^{(5)}(T_2, T_1)$ and its double Fourier transformation for the LL model (a) and (a′) ($\zeta = 1.0\omega_0$), and for the SL model (b) and (b′) ($\zeta' = 0.5\omega_0$ and $T = 150\,\mathrm{K}$).

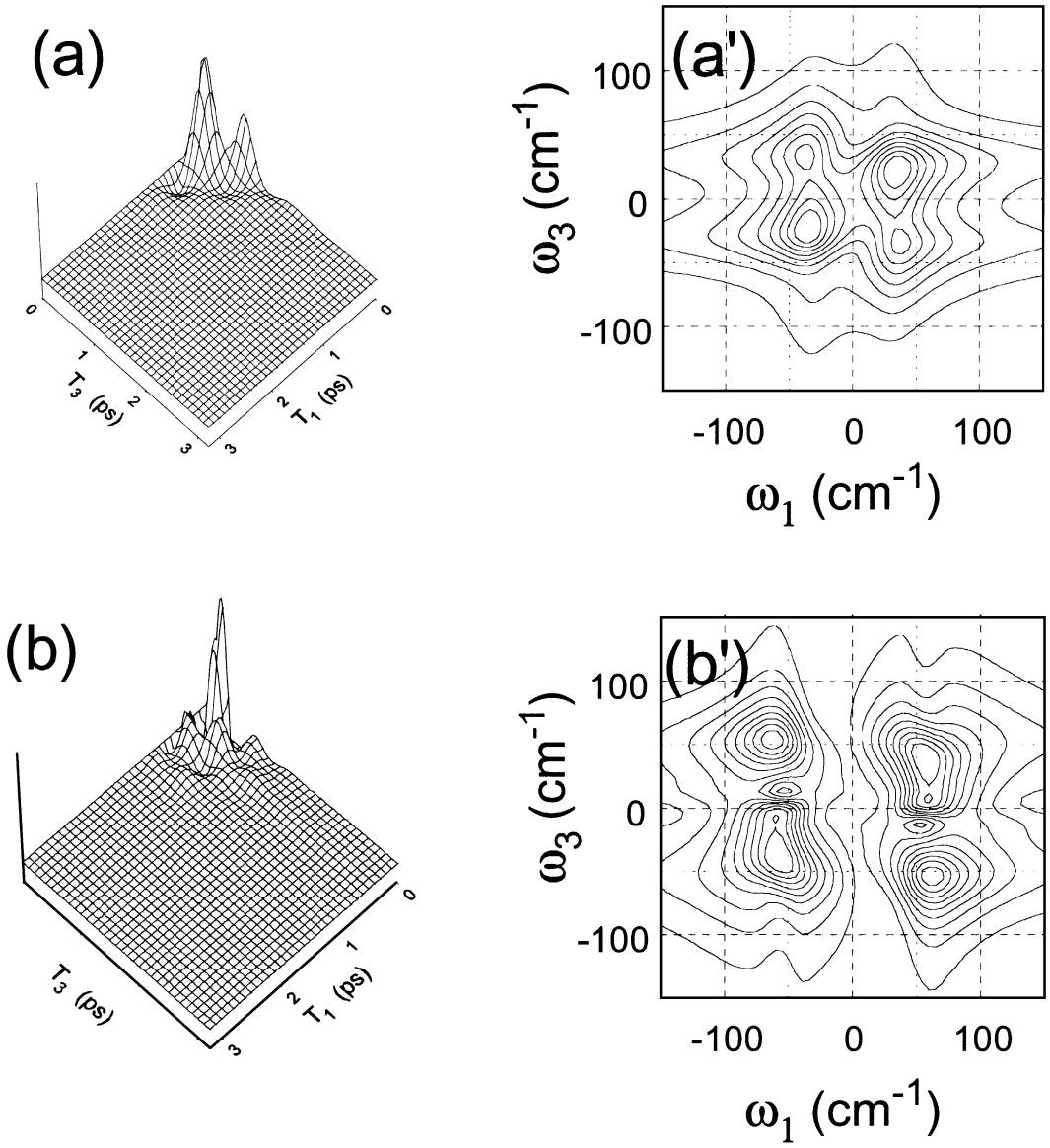

Fig. 14. Three-dimensional profile of the seventh-order Raman signal $I^{(7)}(T_1, T_3) = R^{(7)}(T_3, 0, T_1)$ in the SL-model and its double Fourier transformation for the LL model (a) and (a′) ($\zeta = 1.0\omega_0$), and the SL model (b) and (b′) ($\zeta' = 0.5\omega_0$ and $T = 150\,\mathrm{K}$).

for level-dependent homogeneous pure dephasing. When the system and the bath are strongly coupled, the 2D Raman response becomes highly asymmetric. The signal decays rapidly as function of the first propagation time, which is assigned to very effective phase relaxation. Along the second time variable the decay is an order of magnitude slower which is attributed to a Liouville space path way involving a population during the second propagation time. The impulsive 2D Raman response of molecular liquids reported so far cannot be explained by this model. In the experimental data the tail is along the first propagation time whereas it is along the second propagation time in the simulations.[11] The experimental signal is attributed to strong mode coupling, predominant contributions of Γ_{LL}, and to other scattering mechanisms.

Due to the nonlinear coordinate dependence of the damping operator Γ_{SL} the population and phase relaxation becomes level-dependent in the SL model. Therefore, a finite seventh-order response is predicted for a harmonic oscillator with linear coordinate dependence of the polarizability α_1. In the LL model this response vanishes due to perfect destructive interference of the involved Liouville space path ways.[62] This indicates that even the signal is very weak in the fifth-order experiment, due to the small nonlinearlity α_2, one may detect the signal in the seventh-order experiment if the system is described by the SL model. For weak coupling the response shows oscillations with the frequency of the unperturbed system while for strong coupling the frequency becomes higher. This effect is attributed to a level dependent effective frequency Ω.

For the calculations presented here it was assumed that the heat bath induces Gaussian white noise. Therefore, the memory time of the fluctuations is zero and there is no echo feature predicted, neither in the fifth-nor

in the seventh-order Raman response. Memory effects can, in principle, be induced by a different spectral density $J_{\rm SL}(\omega)$ of the heat bath. As was shown by Tanimura and coworkers[75-79] it is possible to derive a hierarchy of coupled equations of motion for a Gaussian-Markovian heat bath. Up to now this approach, which explicitly includes memory effects, has only been applied to the LL model. The extension of this so-called doctor equation to the SL model is very interesting since it allows for a direct comparison with the stochastic model by Anderson and Kubo.[65] In contrast to the latter case the damping operator in the SL model does depend explicitly on temperature and, therefore, partly bridges the gap between the stochastic and the dynamic theories. As demonstrated here the damping operator $\Gamma_{\rm SL}$ yields reasonable predictions of the third-, fifth-, and seventh-order Raman response for the special case of Gaussian white noise; the extension to Gaussian-Markovian noise should be possible as well.

The SL model with colored noise describes nonresonant interaction of a quantum system coupled to a bath with a finite memory time. It can, for instance, represent the intramolecular vibrational dynamics of a set of inhomogeneously distributed solute molecules, which are subjected to inertial interactions with the surrounding solvent molecules (solvation). By changing the characteristics of the noise spectrum it is possible to continuously interpolate between the present analysis of Gaussian-white case (homogeneous limit), where the fluctuations induced by the bath are very fast compared to the characteristic time of the system, and the situation where the vibrational frequencies of the solute molecules can be described by a static statistical distribution (inhomogeneous limit). Thus, by using the SL model with colored noise, we can study a distribution of solvent molecules from homogeneous to inhomogeneous broadening by changing a single parameter as will be demonstrated in the next paper.[101]

Acknowledgments

The investigations were supported by the Grand-in-Aid on Priority Area of "Chemical Reaction Dynamics in Condensed Phases" (10206210), the Grand-in-Aid for Scientific research (B), Shimazu Science Foundation, and by the Netherlands Foundations for Chemical Research (SON) and Physical Research (FOM) with financial aid from the Netherlands Organization for the Advancement of Science (NWO). One of us (T.S.) wants to thank the Van Dierendonck foundation of the Dutch Physical Society, Section Atomic Physics and Quantumelectronics, for a travel grant.

Appendix: Derivation of the Quantum Fokker-Planck Equation for Square-Linear Interaction

For the derivation of the quantum Fokker-Planck equation in the SL model we first consider the time evolution of the reduced density matrix, which can be represented by a functional integral:[67, 68, 71, 72]

$$\rho(Q_f,Q'_f;t)=\int_{-\infty}^{\infty}\mathrm{d}Q_i\int_{-\infty}^{\infty}\mathrm{d}Q'_i\int_{Q(t_i)=Q_i}^{Q(t)=Q_f}\mathrm{D}[Q(t)]\int_{Q'(t_i)=Q'_i}^{Q'(t)=Q'_f}\mathrm{D}[Q'(t)]$$
$$\times\exp\left\{\frac{\mathrm{i}}{\hbar}(S[Q]-S[Q'])\right\}\exp\left\{-\frac{1}{\hbar}\Phi[Q,Q']\right\}\rho(Q_i,Q'_i;0), \tag{A·1}$$

where the two real time path integrals are over all paths $Q(s)$, $Q'(s)$, $0\le s\le t$ with $Q(0)=Q_i$, $Q'(0)=Q'_i$, $Q(t)=Q_f$ and $Q'(t)=Q_f$ while the outer two integrals are over all possible coordinates of the initial system state Q_i and Q'_i. The path probability is weighted not only by the usual action $S[Q]$ given by:

$$S[Q]=\int_0^t\mathrm{d}s\left(\frac{M}{2}\dot{Q}^2-U'(Q)\right), \tag{A·2}$$

but also by the Feynman-Vernon influence functional, which accounts for the bath-induced relaxation. Note that the counter term in eq. (1) is included in the potential $U(Q)$ and is denoted by $U'(Q)$. For both the LL and the SL model this quantity can be expressed in terms of the influence phase $\Phi[Q,Q']$, which in the SL model is given by:

$$\Phi[Q,Q']=\int_0^t\mathrm{d}s\int_0^s\mathrm{d}u[Q^2(s)-Q'^2(s)][Q^2(u)-Q'^2(u)]L_2(s-u)$$
$$+\mathrm{i}\int_0^t\mathrm{d}s\int_0^s\mathrm{d}u[Q^2(s)-Q'^2(s)][Q^2(u)+Q'^2(u)]L_1(s-u) \tag{A·3}$$

The influence of the environment is completely determined by the spectral density $J_{\rm SL}(\omega)$ of the bath oscillators:

$$J_{\rm SL}(\omega)=\pi\sum_{j=1}^{N}\frac{g_j^2}{8m_j\omega_j}\delta(\omega-\omega_j). \tag{A·4}$$

The complex kernel $L(s)=L_2(s)+\mathrm{i}L_1(s)$ can be expressed in terms of $J_{\rm SL}(\omega)$ via:

$$L_2(s)=\int_0^\infty\frac{\mathrm{d}\omega}{\pi}J_{\rm SL}(\omega)\coth\frac{\omega\hbar\beta}{2}\cos\omega s, \tag{A·5}$$

and:

$$L_1(s) = -\int_0^\infty \frac{\mathrm{d}\omega}{\pi} J_{\mathrm{SL}}(\omega) \sin \omega s. \qquad \text{(A·6)}$$

In the LL model the influence phase Φ and the spectral density $J(\omega)$ have to be slightly changed: all Q^2 in eq. (A·3) and $g_j/2$ in eq. (A·4) have to be replaced by Q and c_j, respectively.

For the derivation of the quantum Fokker-Planck equation let us consider eq. (A·1) at a small time instant later, where the system propagated from Q_f and Q'_f to Q and Q', respectively:

$$\rho(Q,Q';t+\varepsilon) = \int_{-\infty}^{\infty}\mathrm{d}Q_i \int_{-\infty}^{\infty}\mathrm{d}Q'_i \int_{Q(t_i)=Q_i}^{Q(t+\varepsilon)=Q_f} \mathrm{D}[Q(t)] \int_{Q'(t_i)=Q'_i}^{Q'(t+\varepsilon)=Q'_f} \mathrm{D}[Q'(t)] \times \exp\left\{\frac{\mathrm{i}}{\hbar}(S[Q]-S[Q'])\right\} \exp\left\{-\frac{1}{\hbar}\Phi[Q,Q']\right\} \rho(Q_i,Q'_i;0). \qquad \text{(A·7)}$$

Note that now the integrals in the expression for the action [eq. (A·2)] and for the influence phase [eq. (A·3)] also run to $t+\varepsilon$ instead of t.

For small the last part of the path integrals, which run from Q_f to Q and from Q'_f to Q', can be split and approximated by a straight line times a normalization constant C. Similarly, the integrals from 0 to $t+\varepsilon$ can be split into two integrals running from 0 to t and from t to $t+\varepsilon$, respectively. The latter integrals can be approximated by times the integrand at $t+\varepsilon$; moreover, it is a good approximation to replace derivatives around $t+\varepsilon$ by finite differences, *e.g.*, $\partial Q/\partial t$ by $(Q-Q_f)/\varepsilon$. The last equation can then be rewritten as:

$$\begin{aligned}\rho(Q,Q';t+\varepsilon) = \frac{1}{C^2}\int_{-\infty}^{\infty}\mathrm{d}Q_i \int_{-\infty}^{\infty}\mathrm{d}Q'_i \int_{-\infty}^{\infty}\mathrm{d}Q_f \int_{-\infty}^{\infty}\mathrm{d}Q'_f \int_{Q(t_i)=Q_i}^{Q(t)=Q_f} \mathrm{D}[Q(t)] \int_{Q'(t_i)=Q'_i}^{Q'(t)=Q'_f} \mathrm{D}[Q'(t)] \\ \times \exp\left\{\frac{\mathrm{i}M}{2\hbar\varepsilon}[(Q-Q_f)^2-(Q'-Q'_f)^2]\right\} \exp\left\{-\frac{\mathrm{i}\varepsilon}{\hbar}[U'(Q)-U'(Q')]\right\} \\ \times \exp\left\{-\frac{\varepsilon}{\hbar}(Q^2-Q'^2)\int_0^{t+\varepsilon}\mathrm{d}s[Q^2(s)-Q'^2(s)]L_2(t+\varepsilon-s)\right\} \\ \times \exp\left\{-\frac{\mathrm{i}\varepsilon}{\hbar}(Q^2-Q'^2)\int_0^{t+\varepsilon}\mathrm{d}s[Q^2(s)+Q'^2(s)]L_1(t+\varepsilon-s)\right\} \\ \times \exp\left\{\frac{\mathrm{i}}{\hbar}(S[Q]-S[Q'])\right\} \exp\left\{-\frac{1}{\hbar}\Phi[Q,Q']\right\} \rho(Q_i,Q'_i;0). \qquad \text{(A·8)}\end{aligned}$$

For small ε almost all exponents are expanded up to first order in ε-except the first exponent, which rapidly oscillates as $\varepsilon \to 0$. It can be shown[71] that only the parts with $Q-Q_f \propto \varepsilon^{1/2}$ and $Q'-Q'_f \propto \varepsilon^{1/2}$ will yield a finite contribution since the exponent hardly changes in this range:

$$\begin{aligned}\rho(Q,Q';t+\varepsilon) = \frac{1}{C^2}\int_{-\infty}^{\infty}\mathrm{d}Q_i \int_{-\infty}^{\infty}\mathrm{d}Q'_i \int_{-\infty}^{\infty}\mathrm{d}Q_f \int_{-\infty}^{\infty}\mathrm{d}Q'_f \int_{Q(t_i)=Q_i}^{Q(t)=Q_f} \mathrm{D}[Q(t)] \int_{Q'(t_i)=Q'_i}^{Q'(t)=Q'_f} \mathrm{D}[Q'(t)] \\ \times \exp\left\{\frac{\mathrm{i}M}{2\hbar\varepsilon}[(Q-Q_f)^2-(Q'-Q'_f)^2]\right\} \\ \times \left[1-\frac{\mathrm{i}\varepsilon}{\hbar}[U'(Q)-U'(Q')] - \frac{\varepsilon}{\hbar}(Q^2-Q'^2)\int_0^{t+\varepsilon}\mathrm{d}s[Q^2(s)-Q'^2(s)]L_2(t+\varepsilon-s)\right. \\ \left. -\frac{\mathrm{i}\varepsilon}{\hbar}(Q^2-Q'^2)\int_0^{t+\varepsilon}\mathrm{d}s[Q^2(s)+Q'^2(s)]L_1(t+\varepsilon-s)\right] \\ \times \exp\left\{\frac{\mathrm{i}}{\hbar}(S[Q]-S[Q'])\right\} \exp\left\{-\frac{1}{\hbar}\Phi[Q,Q']\right\} \rho(Q_i,Q'_i;0). \qquad \text{(A·9)}\end{aligned}$$

The last two terms in the big squared brackets can be rearranged by introducing the function;

$$\bar{L}_1(s) = 2\int_0^\infty \frac{\mathrm{d}\omega}{\pi}\frac{J_{\mathrm{SL}}(\omega)}{\omega}\cos\omega s. \qquad \text{(A·10)}$$

This function is proportional to the correlation function of the collective bath coordinate.[71] From the definition of $L_1(s)$ in eq. (A·6) it is directly evident that $\mathrm{d}\bar{L}_1/\mathrm{d}s = 2L_1(s)$ holds. Using this identity and the relation $\bar{L}_1(0) = \mu$ the last two terms in the big squared brackets of eq. (A·9) can be replaced by:

$$-\frac{\mathrm{i}\varepsilon}{2\hbar}(Q^2-Q'^2)\frac{\mathrm{d}}{\mathrm{d}(t+\varepsilon)} \times \int_0^{t+\varepsilon}\mathrm{d}s[Q^2(s)+Q'^2(s)]\bar{L}_1(t+\varepsilon-s). \qquad \text{(A·11)}$$

For Gaussian white noise the spectral density $J_{\mathrm{SL}}(\omega)$ is given by eq. (3), the corresponding correlation function of the collective bath coordinate is proportional to a delta function:

$$\bar{L}_1(s) = 2M\zeta_{\mathrm{SL}}\delta(s). \tag{A·12}$$

In the high temperature limit $\coth(\hbar\beta\omega/2) \approx 2/\hbar\beta\omega$ and the real part of the kernel $L_2(s)$ is now given by, cf. the definition eq. (A·5):

$$\bar{L}_2(s) = \frac{2M\zeta_{\mathrm{SL}}}{\beta\hbar}\delta(s). \tag{A·13}$$

Using the above relations the expression for $\rho(q, q', t+\varepsilon)$ can be simplified to:

$$\begin{aligned}
&\rho(Q, Q'; t+\varepsilon) \\
&\quad = \frac{1}{C^2}\int_{-\infty}^{\infty}\mathrm{d}Q_f\int_{-\infty}^{\infty}\mathrm{d}Q'_f \\
&\qquad \times \exp\left\{\frac{\mathrm{i}M}{2\hbar\varepsilon}[(Q-Q_f)^2-(Q'-Q'_f)^2]\right\} \\
&\qquad \times \left[1-\frac{\mathrm{i}\varepsilon}{\hbar}[U(Q)-U(Q')]-\frac{M\zeta_{\mathrm{SL}}}{\hbar^2\beta}(Q^2-Q'^2)^2\right. \\
&\qquad \left.-\frac{M\mathrm{i}\zeta_{\mathrm{SL}}\varepsilon}{\hbar}(Q^2-Q'^2)(Q\dot{Q}+Q'\dot{Q}')\right]\rho(Q_f, Q'_f; t).
\end{aligned} \tag{A·14}$$

Now we introduce the new variables $x = Q - Q_f$ and $x' = Q' - Q'_f$ and use the approximations $\partial Q/\partial t \approx x/\varepsilon$ and $\partial Q'/\partial t \approx x'/\varepsilon$. The integrals over Q_f and Q'_f can be transformed into integrals over x and x'. The density matrices $\rho(Q, Q'; t+\varepsilon)$ and $\rho(Q_f, Q'_f; t) = \rho(Q-x, Q'-x'; t)$ are also expanded up to first order in ε. Remember that x and x' are of the order $\varepsilon^{1/2}$ as was explained above. In zeroth order of epsilon the last equation yields the normalization constant $C^2 = 2\pi\varepsilon\hbar/M$. In first order we find the equation of motion for the reduced density matrix in coordinate representation:

$$\begin{aligned}
\frac{\partial\rho}{\partial t} &= -\frac{\hbar}{2M\mathrm{i}}\left(\frac{\partial^2\rho}{\partial Q^2}-\frac{\partial^2\rho}{\partial Q'^2}\right)-\frac{\mathrm{i}}{\hbar}(U(Q)-U(Q'))\rho \\
&\quad -\frac{M\zeta_{\mathrm{SL}}}{\hbar^2\beta}(Q^2-Q'^2)^2\rho \\
&\quad -\zeta_{\mathrm{SL}}(Q^2-Q'^2)\left(Q\frac{\partial\rho}{\partial Q}-Q'\frac{\partial\rho}{\partial Q'}\right).
\end{aligned} \tag{A·15}$$

In an operator representation this equation reads:

$$\begin{aligned}
\frac{\partial\hat{\rho}}{\partial t} &= -\frac{\mathrm{i}}{\hbar}\left[\frac{1}{2M}\hat{P}^2+U(\hat{Q}),\hat{\rho}\right]-\frac{\mathrm{i}\zeta_{\mathrm{SL}}}{\hbar}(\hat{Q}^3\hat{P}\hat{\rho}+\hat{Q}^2(\hat{\rho}\hat{P})\hat{Q} \\
&\quad -\hat{Q}(\hat{P}\hat{\rho})\hat{Q}^2-(\hat{\rho}\hat{P})\hat{Q}^3)-\frac{M\zeta_{\mathrm{SL}}}{\beta\hbar^2}[\hat{Q}^2,[\hat{Q}^2,\hat{\rho}]].
\end{aligned} \tag{A·16}$$

Finally, this expression is transformed into the Wigner representation, which was introduced in §2, see in particular eq. (5). The action of a function of operators onto the density matrix is transformed to the corresponding Wigner space expression via the relations:[92]

$$\begin{aligned}
A(\hat{P},\hat{Q})\hat{\rho} &\to A\left(P+\frac{\hbar}{2\mathrm{i}}\frac{\partial}{\partial R}, R-\frac{\hbar}{2\mathrm{i}}\frac{\partial}{\partial P}\right)W(P,R), \\
\hat{\rho}A(\hat{P},\hat{Q}) &\to A\left(P-\frac{\hbar}{2\mathrm{i}}\frac{\partial}{\partial R}, R+\frac{\hbar}{2\mathrm{i}}\frac{\partial}{\partial P}\right)W(P,R),
\end{aligned} \tag{A·17}$$

which directly results in the quantum Fokker-Planck equation, see eq. (6) with the damping operator as defined in eq. (10).

1) G. R. Fleming: *Chemical Applications of Ultrafast Spectroscopy* (Oxford University Press, New York 1986).
2) P. C. Becker, R. L. Fork, C. H. Brito Cruz, J. P. Gordon and C. V. Shank: Phys. Rev. Lett. **60** (1988) 2462.
3) K. A. Nelson and E. P. Ippen: Adv. Chem. Phys. **75** (1989) 1.
4) E. T. J. Nibbering, D. A. Wiersma and K. Duppen: Phys. Rev. Lett. **66** (1991) 2464.
5) S. Mukamel: *Principles of Nonlinear Optical Spectroscopy* (Oxford University Press, Oxford 1995).
6) W. P. de Boeij, M. S. Pshenichnikov and D. A. Wiersma: Ann. Rev. Phys. Chem. **49** (1998) 99.
7) N. Bloembergen: *Nonlinear Optics* (Benjamin, Boston 1965).
8) Y. Tanimura and S. Mukamel: J. Chem. Phys. **99** (1993) 9496.
9) T. Steffen, J. T. Fourkas and K. Duppen: J. Chem. Phys. **105** (1996) 7364.
10) K. Tominaga and K. Yoshihara: Phys. Rev. Lett. **74** (1995) 3061.
11) T. Steffen and K. Duppen: Phys. Rev. Lett. **76** (1996) 1224.
12) A. Tokmakoff, M. J. Lang, D. S. Larsen, G. R. Fleming, V. Chernyak and S. Mukamel: Phys. Rev. Lett. **79** (1997) 2702.
13) J. E. Ivanecky and J. C. Wright: Chem. Phys. Lett. **206** (1993) 437.
14) D. J. Ulness, J. C. Kirkwood and A. C. Albrecht: J. Chem. Phys. **108** (1998) 3897.
15) D. A. Blank, L. J. Kaufman and G. R. Fleming: J. Chem. Phys. **111** (1999) 3105.
16) M. Cho, D. A. Blank, J. Sung and G. R. Fleming: J. Chem. Phys. **112** (2000) 2082.
17) T. l. C. Jansen, J. G. Snijders and K. Duppen: J. Chem. Phys. **113** (2000) 307.
18) V. Astinov, K. Kubarych, C. J. Milne and R. J. D. Miller: Opt. Lett. **25** (2000) 853.
19) V. Astinov, K. Kubarych, C. J. Milne and R. J. D. Miller: Chem. Phys. Lett. in press.
20) D. A. Blank, L. J. Kaufman and G. R. Fleming: J. Chem. Phys. **113** (2000) 771.
21) M. Cho, K. Okumura and Y. Tanimura: J. Chem. Phys. **108** (1998) 1326.
22) M. Cho: J. Chem. Phys. **111** (1999) 10587.
23) J. C. Kirkwood and A. C. Albrecht and D. J. Ulness: J. Chem. Phys. **111** (1999) 253.
24) J. C. Kirkwood, A. C. Albrecht, D. J. Ulness and M. J. Stimson: J. Chem. Phys. **111** (1999) 272.
25) W. Zhao and J. C. Wright: Phys. Rev. Lett., **83** (1999) 1950.
26) W. Zhao and J. C. Wright: J. Am. Chem. Soc., **121** (1999) 10994.
27) W. Zhao and J. C. Wright: Phys. Rev. Lett. **84** (2000) 1411.
28) X. D. Zhu and Y. R. Shen: Appl. Phys. **B50** (1990) 535.
29) P. Guyoy-Sionnest: Phys. Rev. Lett. **66** (1991) 1489.
30) A. Tokmakoff, A. S. Jwok, R. S. Urdahl, R. S. Francis and M. D. Fayers: Chem. Phys. Lett. **234** (1995) 289.
31) P. Hamm, M. Lim and R. E. Hohstrasser: Phys. Rev. Lett. **81** (1999) 5326.
32) S. Mukamel, A. Piryatinski and V. Chernyak: J. Chem. Phys. **110** (1999) 1711.
33) K. Park and M. Cho: J. Chem. Phys., **109** (1998) 10559.

34) P. Hamm, M. Lim, W. F. DeGrado and R. M. Hochstrasser: Proc. Natl. Acad. Sci. U.S.A., **96** (1999) 2036.
35) M. Cho: Phs. Rev. B **61** (2000) 023406.
36) R. F. Loring and S. Mukamel: J. Chem. Phys. **83** (1985) 2116.
37) D. Vanden Bout, L. J. Muller and M. Berg: Phys. Rev. Lett. **43** (1991) 3700.
38) R. Inaba, K. Tominaga, M. Tasumi, K. A. Nelson and K. Yoshihara: Chem. Phys. Lett. **211** (1993) 183.
39) T. W. Mossberg, R. Kachru, S. R. Hatmann and A. M. Flusberg: Phys. Rev. A **20** (1979) 1976.
40) D. A. Wiersma and K. Duppen: Science **237** (1987) 1147.
41) J.-Y. Bigot, M. T. Portella, R. W. Schoenlein, C. J. Bardeen, A. Migus and C. V. Shank: Phys. Rev. Lett. **66** (1991) 1138.
42) S. M. G. Faeder and D. M. Jonas: J. Phys. Chem. A **103** (1999) 10489.
43) Y. Tanimura and K. Okumura: J. Chem. Phys. **106** (1997) 2078.
44) A. Tokmakoff and G. R. Fleming: J. Chem. Phys. **106** (1997) 2569.
45) S. Saito and I. Ohmine: J. Chem. Phys. **108** (1998) 240.
46) K. Okumura and Y. Tanimura: J. Chem. Phys. **106** (1997) 1687.
47) K. Okumura and Y. Tanimura: J. Chem. Phys. **107** (1997) 2267.
48) K. Okumura and Y. Tanimura: Chem. Phys. Lett. **277** (1997) 159.
49) Y. Tanimura: Chem. Phys. **233** (1998) 217.
50) V. Chernyak and S. Mukamel: J. Chem. Phys. **108** (1998) 5812.
51) S. Hahn, K. Park and M. Cho: J. Chem. Phys. **111** (1999) 4121.
52) K. Park, M. Cho, S. Hahn and D. Kim: J. Chem. Phys., **111** (1999) 4131.
53) K. Park and M. Cho: J. Chem. Phys. **112** (2000) 10496.
54) K. Okumura and Y. Tanimura: Chem. Phys. Lett. **278** (1997) 175.
55) R. L. Murry, J. T. Fourkas and T. Keyes: J. Chem. Phys. **109** (1998) 7913.
56) T. Keys and J. T. Fourkas: J. Chem. Phys. **112** (2000) 287.
57) K. Okumura, A. Tokmakoff and Y. Tanimura: J. Phys. Chem. **111** (1999) 492
58) S. Hahn, K. Kwak and M. Cho: J. Chem. Phys. **112** (2000) 4553.
59) M. Cho: J. Chem. Phys. **111** (1999) 4140.
60) W. T. Pollard and R. A. Friesner: J. Chem. Phys. **100** (1994) 5054.
61) J. S. Bader and B. J. Berne: J. Chem. Phys. **100** (1994) 8359.
62) J. T. Fourkas, H. Kawashima and K. A. Nelson: J. Chem. Phys. **103** (1995) 4393.
63) R. A. Farrer, B. J. Loughnane, L. A. Deschenes and J. T. Fourkas: J. Chem. Phys. **106** (1997) 6901.
64) R. Kubo: Adv. Chem. Phys. **15** (1969) 101.
65) R. Kubo, M. Toda and N. Hashitsume: *Statistical Physics, Vol. 2* (Springer, Berlin 1985).
66) T. Steffen and K. Duppen: Chem. Phys. **233** (1998) 267.
67) R. P. Feynman and F. L. Vernon: Ann. Phys. **24** (1963) 118.
68) H. Grabert, P. Schramm and G.-L. Ingold: Phys. Rep. **168** (1988) 115.
69) U. Weiss: *Quantum Dissipative Systems*, 2nd ed. (World Scientific, Singapore 1999).
70) Y. Tanimura and S. Mukamel: Phys. Rev. E **47** (1993) 118.
71) A. O. Caldeira and A. J. Leggett: Physica A **121** (1983) 587.
72) L. D. Chang and D. Waxman: J. Phys. C **18** (1985) 5873.
73) K. Okumura and Y. Tanimura: J. Chem. Phys. **105** (1996) 7294.
74) Y. Tanimura and S. Mukamel: J. Chem. Phys. **101** (1994) 3049.
75) Y. Tanimura and R. Kubo: J. Phys. Soc. Jpn. **58** (1989) 101.
76) Y. Tanimura and R. Kubo: J. Phys. Soc. Jpn. **58** (1989) 1199.
77) Y. Tanimura and P. Wolynes: Phys. Rev. A **43** (1991) 4131.
78) Y. Tanimura and P. Wolynes: J. Chem. Phys. **96** (1992) 8485.
79) Y. Tanimura and Y. Maruyama: J. Chem. Phys. **107** (1997) 1779.
80) Y. Maruyama and Y. Tanimura: Chem. Phys. Lett. **292** (1998) 28.
81) C. Meier and D. J. Tannor: J. Chem. Phys. **111** (1999) 3365.
82) Y. J. Yan: Phys. Rev. A**58** (1998) 2721.
83) O. Kuhn, Y. Zhao, F. Shuang and Y. J. Yan: J. Chem. Phys. **112** (2000) 6104.
84) D. W. Oxtoby: Adv. Chem. Phys. **40** (1979) 1.
85) D. W. Oxtoby and S. A. Rice: Chem. Phys. Lett. **42** (1976) 1.
86) P. A. Madden and R. M. Lynden-Bell: Chem. Phys. Lett. **38** (1976) 163.
87) D. J. Diestler: Chem. Phys. Lett. **39** (1977) 39.
88) D. C. Knauss and R. S. Wilson: Chem. Phys. **19** (1977) 341.
89) S. Bratos and G. Tarjus: Phys. Rev. A **24** (1981) 1591.
90) K. Okumura and Y. Tanimura: Phys. Rev. E **56** (1997) 2747.
91) E. Wigner: Phys. Rev. **40** (1932) 749.
92) R. Kubo: J. Phys. Soc. Jpn. **19** (1964) 2127.
93) M. Hillery, R. F. O'Connel, M. O. Scully and E. P. Wigner: Phys. Rep. **106** (1984) 121.
94) W. R. Frensley: Rev. Mod. Phys. **62** (1990) 745.
95) D. McMorrow and W. T. Lotshaw: Chem. Phys. Lett. **174** (1990) 85.
96) D. McMorrow and W. T. Lotshaw: J. Phys. Chem. **95** (1991) 10395.
97) D. McMorrow: Opt. Commun. **86** (1991) 236.
98) A. Tokmakoff, M. J. Lang, D. S. Larsen and G. R. Fleming: **272** (1997) 48.
99) L. J. Muller, D. Vanden Bout and M. Berg: J. Chem. Phys. **99** (1993) 810.
100) M. Berg and D. Vanden Bout: Acc. Chem. Res. **30** (1997) 65.
101) Y. Tanimura and T. Steffen: to be published in J. Phys. Soc. Jpn.